

Fast and Accurate Low-Rank Tensor Completion Methods Based on QR Decomposition and $L_{2,1}$ Norm Minimization

HongBing Zhang, XinYi Liu, HongTao Fan, YaJing Li, Yinlin Ye

Abstract—Recently, tensor complete method has been widely used in multidimensional data recovery, especially in the case of serious lack of data information. The existing tensor complete problem is essentially to solve the tensor rank minimization problem. Among them, the commonly used method to solve the tensor complete problem is to approximate it to solve the problem of minimizing the nuclear norm related to the matrix form or its related improvements to solve. However, it is worth noting that the core calculations of the vast majority of such methods available involve the calculation of the singular value decomposition (SVD) of the matrix obtained by the expansion of the tensor mode, which will lead to a sharp increase in the computational cost of the problem, and in turn cause the efficiency of the solution to be particularly slow, especially when the tensor data information is very large. Concretely, for a matrix $X \in \mathbb{R}^{m \times n}$, the computational complexity of its singular value decomposition is $O(mn^2)$, and where n is extremely large in practice, i.e., the product of the tensor dimensions except one of the other dimensions. More recently, an Approximate SVD Based on QR Decomposition (CSVD-QR) [1] method for matrix complete problem is presented, whose computational complexity is $O(r^2(m+n))$, which is mainly due to that r is far less than $\min\{m, n\}$, where r represents the largest number of singular values of matrix X . What is particularly interesting is that after replacing the nuclear norm with the $L_{2,1}$ norm proposed based on this decomposition, as the upper bound of the nuclear norm, when the intermediate matrix D in its decomposition is close to the diagonal matrix, it will converge to the nuclear norm, and is exactly equal, when the D matrix is equal to the diagonal matrix, to the nuclear norm, which ingeniously avoids the calculation of the singular value of the matrix. To the best of our knowledge, there is no literature to generalize and apply it to solve tensor complete problems. Inspired by this, in this paper we propose a class of tensor minimization model based on $L_{2,1}$ norm and CSVD-QR method for the tensor complete problem, which is convex and therefore has a global minimum solution. Subsequently, in order to further improve the accuracy of our model, a TLNMTV model was proposed by adding TV regularization terms, which not only improves the use of local sparse prior information, but also greatly promotes the restoration effect on local detail information. Finally, three multidimensional data experiments of hyperspectral images, magnetic resonance images, and color video images are used to compare the proposed method with

state-of-the-art methods to illustrate the rapidity and efficiency of the proposed method. The experimental results show that when solving the tensor complete problem, the TLNM method takes extremely short time compared with other methods while maintaining high image quality indicators and fairly good visual effects. In particular, for hyperspectral images its image visual effect is the best among all methods when the sampling rate is 2.5%. Meanwhile, the quantitative picture quality indices (PQIs) and visual effects of the TLNMTV method are the most excellent, especially in terms of detail information extraction.

Index Terms—Tensor nuclear norm, $L_{2,1}$ norm, alternating direction method of multipliers (ADMM), low-rank (LR) tensor completion, an approximate SVD based on QR Decomposition (CSVD-QR).

I. INTRODUCTION

LOW-RANK tensor completion (LRTC) has received, especially when dealing with extremely high-dimensional data, extensive attention in recent years, and is widely used in color picture and video processing, magnetic resonance images, hyperspectral image [2], pattern recognition [3], [4] face modeling and analysis [5] and other fields. However, due to various objective factors in real life, such as poor imaging acquisition conditions of visual data, or severe data damage during transmission, the obtained data is incomplete or severely damaged. This will promote the research of tensor complete [6] and tensor robustness principal component analysis [7] with the acquired data, especially how to make use of the internal structure information between the obtained observation data and the lost data to achieve tensor complete will become particularly important.

As is known to all, tensors are higher-order forms of matrices and vectors, but the existing strategies for solving matrix complete problems and other techniques cannot be directly applied to solving tensor complete problems. One essential reason for this is that the definition of tensor rank is not unique. In the past few years, many definitions of the rank of tensors have been proposed according to the different ways in which the tensors are decomposed, such as CANDECOMP/PARAFAC (CP) rank [8], [9] generated by CP decomposition [10], Tucker-rank generated by Tucker decomposition [11], [12], and tube rank and multi-rank based on tensor products [13], [14], etc. However, the obtained different ranks have their own defects. For example, the calculation of the rank of tensor CP is NP-hard [15]; the determination of Tucker rank [16], [17] requires the operation of the mode n unfolding and folding of one tensor, which will cause the

This work was supported by the National Natural Science Foundation of China (Nos. 11701456, 11801452, 11571004), Fundamental Research Project of Natural Science in Shaanxi Province General Project (Youth) (Nos. 2019JQ-415, 2019JQ-196), the Initial Foundation for Scientific Research of Northwest A&F University (Nos. 2452017219, 2452018017), and Innovation and Entrepreneurship Training Program for College Students of Shaanxi Province (S201910712132).

H. Zhang, X. Liu, H. Fan, Y. Li and Y. Ye are with the College of Science, Northwest A&F University, Yangling, Shaanxi 712100, China (e-mail: zhanghb@nwfau.edu.cn; Lxy6x1@163.com; fanht17@nwfau.edu.cn; hliya-jing@163.com; 13314910376@163.com).

curse of dimensionality; the multi-rank and tube rank based on t-SVD decomposition induced by tensor product only apply to third-order tensors due to the current limitations of tensor product. Mathematically, low-rank tensor complete problems mentioned above can be expressed in the following form:

$$\min_{\mathcal{X}} \text{rank}(\mathcal{X}), \quad s.t. \quad \mathcal{X}_{\Omega} = \mathcal{T}_{\Omega} \quad (1)$$

where \mathcal{T} and \mathcal{X} are the incomplete and completed tensors, respectively, Ω denotes the indices of the observed elements of \mathcal{T} , $\text{rank}(\mathcal{X})$ indicates the rank of tensor \mathcal{X} , conditions to be met $\mathcal{X}_{\Omega} = \mathcal{T}_{\Omega}$ mean that the entries of \mathcal{X} should agree with \mathcal{T} in Ω . However, it is well known that the rank of the tensor with respect to \mathcal{X} is not a convex function as is the rank of the matrix. In this regard, Liu et al. [18] turn to use the convex envelope nuclear norm of the rank function to replace it, and propose a tensor nuclear norm minimization method to solve such problems, especially for image restoration problems

$$\min_{\mathcal{X}} \|\mathcal{X}\|_*, \quad s.t. \quad \mathcal{X}_{\Omega} = \mathcal{T}_{\Omega} \quad (2)$$

where $\|\mathcal{X}\|_* = \sum_{n=1}^N \alpha_n \|\mathbf{X}_{(n)}\|_*$ (α_n denotes a constant satisfying $\alpha_n \geq 0$ and $\sum_{n=1}^N \alpha_n = 1$). Such as the above model (2) has a relatively ideal effect in image global information restoration, while the extraction performance of local information is very insufficient, which is far from meeting the requirements of the actual image restoration application, especially the high-dimensional image restoration problem. In view of this, a local piece-wise smoothness prior is employed to achieve the regularization of the image recovery, and a large class of total variation (TV) minimization method [19] is proposed and applied to image processing and pattern recognition [12], [20], [21], [22]. Generally, for the tensor complete problem, the TV term is usually included in the LR framework to jointly represent the local piece-wise continuity and global LR structure along different dimensions [23], [24], [25], [26], thus greatly improving the local information effect of the model. The specific model is shown as follows:

$$\min_{\mathcal{X}} \|\mathcal{X}\|_* + \lambda \|\mathcal{X}\|_{TV}, \quad s.t. \quad \mathcal{X}_{\Omega} = \mathcal{T}_{\Omega} \quad (3)$$

where $\|\mathcal{X}\|_{TV}$ is TV regularization term, and the parameter $\lambda > 0$ is used to balance the relationship between the nuclear norm and the regularization term. Due to the large amount of data contained in tensor, the calculation of TV regularization term costs a lot of time. Therefore, the method of introducing TV regularization term improves the quality of image restoration at the cost of computing speed.

In order to solve the nuclear norm minimization problem of (2) and (3), it is necessary to calculate the SVD of each mode unfolding matrix in each iteration. As a representation of multi-dimensional data, a tensor contains a large number of elements, which makes the dimension of the unfolding matrix of each mode generally large. Therefore, it takes a long time to calculate the SVD of the unfolding matrix, which in turn reduces the overall solution speed, which is extremely unfavorable for practical applications. Recently, Liu et al. proposed a fast and accurate matrix completion method in [1]. To the best of our knowledge, it has not been introduced and is used to solve tensor complete problems. Inspired by the above

method, we propose a method that does not require calculating SVD to solve low-rank tensor model, which greatly reduces the computational cost of the existing advanced methods and further improves the efficiency of the solution. Furthermore, in order to make full use of local prior information and improve the accuracy of tensor complete, a method with TV is proposed. To summarize, our proposed method takes these issues into consideration and the main contributions can be highlighted as follows.

1) : In order to improve the solving speed of the low-rank tensor complete problem model, we use, instead of singular value decomposition of the matrix, the Computing an Approximate SVD Based on Qatar Riyal (QR) Decomposition (CSVD-QR) method, which does not need to calculate the singular value of the matrix related and the time required is much less than those available methods based on SVD decomposition. In addition, we first use the $L_{2,1}$ norm, which is not only the upper bound of the nuclear norm, but also can converge to the nuclear norm when the decomposition is based on CSVD-QR, to replace the commonly used nuclear norm to solve the low-rank tensor complete problem. In particular, when the factor matrix D in the CSVD-QR decomposition LDR is diagonal matrix, the $L_{2,1}$ norm happens to be the nuclear norm. Therefore, it not only avoids the SVD decomposition, but also effectively mitigates the double effects of calculation efficiency caused by solving the kernel norm minimization problem based on the SVD decomposition, which further greatly reduces the calculation cost and greatly improves the calculation speed.

2) : In this paper, the tensor $L_{2,1}$ norm minimization (TLNM) method is first proposed for the low-rank tensor complete problem. In order to further improve the extraction of local information, we optimize the low-rank tensor completion model (2) and design the tensor $L_{2,1}$ norm minimization method with TV (TLNMTV) to improve the efficiency, that is, the accuracy, of the TLNM. TV regular items need to calculate the local relevant information of each element, our TLNMTV method is bound to sacrifice some speed to improve the image restoration quality.

3) : Three kinds of high-dimensional experimental data (hyperspectral image, magnetic resonance image, color video image) was executed and showed that TLNM greatly enhanced the speed, that is, the required time is the shortest compared with the state-of-the-art methods, while ensuring the superiority of the recovery results. In particular, it is worth mentioning that when the hyperspectral sampling rate is 2.5%, it can still be restored to obtain particularly satisfactory image visual effects. Most importantly, the image quality indicators and visual effects of the TLNMTV method are the most excellent, especially in terms of detail information extraction.

The summary of this article is as follows: Section II, some preliminary knowledge and background of the complete of tensors and matrices are given. The main results, including the proposed model and algorithm, are shown in Section III. The results of extensive experiments and discussion are presented in Section IV. Conclusions are drawn in section V.

II. PRELIMINARIES

This section provides the basic knowledge of the proposed method. Firstly we give the basic tensor notations.

A. Tensor Notations and Definitions

Generally, a lowercase letter and an uppercase letter denote a vector \mathbf{x} and a matrix X . An N th-order tensor is denoted by a calligraphic upper case letter $\mathcal{X} \in \mathbb{R}^{I_1 \times I_2 \times \dots \times I_N}$ and x_{i_1, i_2, \dots, i_N} is its (i_1, i_2, \dots, i_N) -th element. The Frobenius norm of a tensor is defined as $\|\mathcal{X}\|_F = (\sum_{i_1, i_2, \dots, i_N} x_{i_1, i_2, \dots, i_N}^2)^{1/2}$. The inner product of two N th-order tensors \mathcal{Y} and \mathcal{Z} is defined as $\langle \mathcal{Y}, \mathcal{Z} \rangle = \sum_{i_1, i_2, \dots, i_N} y_{i_1, i_2, \dots, i_N} z_{i_1, i_2, \dots, i_N}$, where y_{i_1, i_2, \dots, i_N} and z_{i_1, i_2, \dots, i_N} are the (i_1, i_2, \dots, i_N) -th element of \mathcal{Y} and \mathcal{Z} , respectively.

Definition 1 (Tensor Mode- n Unfolding and Folding [27]): The mode- n unfolding of a tensor $\mathcal{X} \in \mathbb{R}^{I_1 \times I_2 \times \dots \times I_N}$ is denoted as a matrix $\mathbf{X}_{(n)} \in \mathbb{R}^{I_n \times I_1 \dots I_{n-1} I_{n+1} \dots I_N}$. Tensor element (i_1, i_2, \dots, i_N) maps to matrix element (i_n, j) , where

$$j = 1 + \sum_{k=1, k \neq n}^N (i_k - 1)J_k \quad \text{with} \quad J_k = \prod_{m=1, m \neq n}^{k-1} I_m. \quad (4)$$

The mode- n unfolding operator and its inverse are respectively denoted as unfold_n and fold_n , and they satisfy $X = \text{fold}_n(\mathbf{X}_{(n)}) = \text{fold}_n(\text{unfold}_n(X))$.

Definition 2 (The mode- n product of tensor [27]): The mode- n product of tensor $\mathcal{X} \in \mathbb{R}^{I_1 \times I_2 \times \dots \times I_N}$ with matrix $U \in \mathbb{R}^{J_n \times I_n}$ is denoted by $\mathcal{Y} = \mathcal{X} \times_n U$, where $\mathcal{Y} \in \mathbb{R}^{I_1 \times I_2 \times \dots \times I_{n-1} \times J_n \times I_{n+1} \times \dots \times I_N}$. Elementwise, we have

$$\mathcal{Y} = \mathcal{X} \times_n U \quad \Leftrightarrow \quad \mathbf{Y}_{(n)} = U \cdot \text{unfold}_n(\mathbf{X}_{(n)}). \quad (5)$$

Definition 3 (The $L_{2,1}$ norm of matrix [28]): The $L_{2,1}$ norm of a matrix $M \in \mathbb{R}^{I \times J}$ is denoted by

$$\|M\|_{2,1} = \sum_{j=1}^J \sqrt{\sum_{i=1}^I m_{ij}^2}; \quad (6)$$

where $m_{i,j}$ is the element in the i -th row and j -th column of matrix M .

Definition 4 (Method for Computing an Approximate SVD Based on QR Decomposition (CSVD-QR) [1]): Suppose that $X \in \mathbb{R}^{m \times n}$ is a given real matrix. Such method can compute the largest r ($r \in (0, \min\{m, n\})$) singular values and the corresponding singular vectors of X by QR decompositions directly. Specifically, the method aims to find three matrices, i.e., L , D , and R , such that

$$\|X - LDR\|_F^2 \leq \varepsilon_0 \quad (7)$$

where ε_0 is a positive tolerance. Decompose X into three matrices as follows:

$$X = LDR \quad (8)$$

where $L \in \mathbb{R}^{m \times r}$, $D \in \mathbb{R}^{r \times r}$, $R \in \mathbb{R}^{r \times n}$, $r \in (0, \min\{m, n\})$. The factors L and R denote a column orthogonal matrix and a row orthogonal matrix, respectively. Specifically, they are the orthogonal bases of the columns and rows of X , respectively.

The matrix D does not need to be diagonal. Consequently, a minimization problem is drawn up

$$\min_{L, D, R} \|X - LDR\|_F^2, \quad \text{s.t.} \quad L^T L = I, \quad R R^T = I. \quad (9)$$

The minimization function in (9) is convex to each one of the variables, i.e., L , D , and R , when the remaining two are fixed. Thus, the variables can be alternately updated one by one. Suppose that L_j , D_j , and R_j denote the results of the j th iteration in the alternating method. Let $L_1 = \text{eye}(m, r)$, $D_1 = \text{eye}(r, r)$, and $R_1 = \text{eye}(r, n)$. In the j th iteration, L_{j+1} is updated with fixed D_j and R_j as follows:

$$[Q, T] = \text{qr}(X R_j^T) \quad (10)$$

$$L_{j+1} = Q(q_1, \dots, q_r) \quad (11)$$

where $Q \in \mathbb{R}^{m \times m}$ and $T \in \mathbb{R}^{m \times r}$ are the intermediate variables, and equation (10) indicates that the QR decomposition of $X R_j^T$ is $X R_j^T = QT$. Similarly, R_{j+1} can be updated as follows:

$$[Q, T] = \text{qr}(X^T L_{j+1}) \quad (12)$$

$$R_{j+1} = Q(q_1, \dots, q_r) \quad (13)$$

where $Q \in \mathbb{R}^{n \times n}$ and $T \in \mathbb{R}^{n \times r}$ are the intermediate variables. Since the optimal R is a row orthogonal matrix, we set

$$R_{j+1} = R_{j+1}^T. \quad (14)$$

Finally, D_{j+1} is updated as follows:

$$D_{j+1} = \arg \min_D \|X - L_{j+1} D R_{j+1}\|_F^2 \quad (15)$$

$$= L_{j+1}^T X R_{j+1}^T. \quad (16)$$

According to (12), we have

$$T^T = L_{j+1}^T X Q. \quad (17)$$

Because R_{j+1} is generated by (13) and (14), we have

$$D_{j+1} = T^T (1 \dots r, 1 \dots r). \quad (18)$$

When $\|L_j D_j R_j - X\|_F^2 \leq \varepsilon_0$ or $j > \text{Itmax}$, CSVD-QR stops iterating. Now L_j , D_j , R_j is the result obtained by X through CSVD-QR.

Lemma 1 (The relationship between matrix $L_{2,1}$ norm and nuclear norm [1]): The matrix $A \in \mathbb{R}^{r \times r}$ can be decomposed as follows:

$$A = \sum_{j=1}^r A^j, \quad (19)$$

$$(A^j)_{k,i} = \begin{cases} (A)_{k,j}, & (i = j), \\ 0, & (i \neq j) \end{cases} \quad (20)$$

where $i, j, k = 1, \dots, r$, and $A^j \in \mathbb{R}^{r \times r}$. From (19), we have

$$\|A\|_* = \left\| \sum_{j=1}^r A^j \right\|_* \leq \sum_{j=1}^r \|A^j\|_*. \quad (21)$$

Because $\sum_{j=1}^r \|A^j\|_* = \|A\|_{2,1}$, we have the following conclusion:

$$\|A\|_* \leq \|A\|_{2,1} \quad (22)$$

B. Methods for Matrix Completion

1) *Singular Value Thresholding Method*: A classical nuclear norm based method is the SVT method proposed by Cai et al. [29]. The optimal X can be updated by solving the following problem :

$$\min_X \mu \|X\|_* + \frac{1}{2} \|X - Y\|_F^2. \quad (23)$$

The problem in (23) can be settled by the singular value shrinking operator (SVT) [29] shown in Lemma 2 below.

Lemma 2 (SVT [29]): For each $\mu \geq 0, Y \in \mathbb{R}^{m \times n}$ is a given real matrix, where $Y = U\Lambda V^T$ is the SVD decomposition of Y . The global minimum solution to

$$S_\mu(Y) = \arg \min_X \mu \|X\|_* + \frac{1}{2} \|X - Y\|_F^2 \quad (24)$$

is given by the singular value shrinking operator

$$S_\mu(Y) = U \text{diag}(\Sigma_i(\Lambda_{ii})) V^T \quad (25)$$

where $\Sigma_i(\Lambda_{ii}) = \max\{\Lambda_{ii} - \mu, 0\}$ and $i = 1, \dots, n$.

The SVT method has efficient convergence on a matrix with a strict low-rank structure. However, due to the high cost of SVD iterative computation, its usefulness has been greatly reduced.

2) *$L_{2,1}$ -Norm Minimization Method*: Recently, the $L_{2,1}$ norm was successfully used in low-rank representation [28] to optimize the noise data matrix $L \in \mathbb{R}^{m \times n}$. The optimal L can be updated by solving the minimization problem as follows:

$$\min_L \tau \|L\|_{2,1} + \frac{1}{2} \|L - C\|_F^2 \quad (26)$$

where $C \in \mathbb{R}^{m \times n}$ is a given real matrix and $\tau > 0$. The $L_{2,1}$ - norm of L is defined as Definition 3.

Lemma 3 ($L_{2,1}$ norm minimization solver (LNMS) [1]): The optimal $L(:, j)$ (denoting the j th column of L) of the problem in (26) obeys

$$L(:, j) = \frac{\max\{\|C(:, j)\|_2 - \tau, 0\}}{\|C(:, j)\|_2} C(:, j) \quad (27)$$

where $\|C(:, j)\|_2 = \sqrt{\sum_{i=1}^m C_{ij}^2}$.

We can know from the above two lemmas. The computational complexity of SVT is $O(mn^2)$, where $n < m$. The computational complexity of LNMS is $O(mn)$. It can be seen that the LNMS method requires much less time than the SVT method.

III. THE PROPOSED MODEL AND ALGORITHM

A. Application of $L_{2,1}$ -Norm Minimization and CSVD-QR method to Tensor Completion

This paper aims to investigate a fast and accurate tensor completion method based on $L_{2,1}$ -norm minimization and CSVD-QR method. Firstly, we introduce some auxiliary parameters $\mathcal{M}_n = \mathcal{X}(n = 1, \dots, N)$. Then LRTC problem (2) can be rewritten as:

$$\begin{aligned} \min_{\mathcal{X}} \sum_{n=1}^N \alpha_n \|\mathbf{M}_{n(n)}\|_* \\ \text{s.t. } \{\mathcal{M}_n = \mathcal{X}\}_{n=1}^N, \quad \mathcal{X}_\Omega = \mathcal{T}_\Omega \end{aligned} \quad (28)$$

Due to the matrix form of $\mathbf{M}_{n(n)}$ in its objective function, it can be decomposed into $\mathbf{M}_{n(n)} = L_n D_n R_n$ by the CSVD-QR method, where L_n is a column orthogonal matrix and R_n is a row orthogonal matrix and $D_n \in \mathbb{R}^{r_n \times r_n}$. Because of this, the following conclusions can be obtained:

$$\|\mathbf{M}_{n(n)}\|_* = \|D_n\|_*. \quad (29)$$

Further, the problem (28) is transformed into the following minimization problem :

$$\begin{aligned} \min_{\mathcal{X}} \sum_{n=1}^N \alpha_n \|D_n\|_* \\ \text{s.t. } \{\mathcal{M}_n = \mathcal{X}\}_{n=1}^N, \quad \mathcal{X}_\Omega = \mathcal{T}_\Omega \\ \{\mathbf{M}_{n(n)} = L_n D_n R_n\}_{n=1}^N, \\ L_n^T L_n = I_n, R_n R_n^T = I_n. \end{aligned} \quad (30)$$

It is not difficult to find through observation that although the dimension of D_n matrix is greatly reduced compared with $\mathbf{M}_{n(n)}$ matrix, as the objective function still includes the minimization of kernel norm, the singular value of D_n matrix still needs to be calculated. According to the LNMS method, it is not necessary to calculate the singular value of the correlation matrix when it is replaced by $L_{2,1}$ norm minimization. And from Lemma 1, we know $\|D_n\|_* \leq \|D_n\|_{2,1}$, i.e., the $L_{2,1}$ norm is the upper bound of the nuclear norm, and the $L_{2,1}$ norm can converge to the nuclear norm based on CSVD-QR, which indicates that in this case, the use of $L_{2,1}$ can not only improve the calculation speed, but also ensure the accuracy of the model. At this moment, the problem (30) can be converted into:

$$\begin{aligned} \min_{\mathcal{X}} \sum_{n=1}^N \alpha_n \|D_n\|_{2,1} \\ \text{s.t. } \{\mathcal{M}_n = \mathcal{X}\}_{n=1}^N, \quad \mathcal{X}_\Omega = \mathcal{T}_\Omega \\ \{\mathbf{M}_{n(n)} = L_n D_n R_n\}_{n=1}^N, \\ L_n^T L_n = I_n, R_n R_n^T = I_n. \end{aligned} \quad (31)$$

Hereafter, the tensor $L_{2,1}$ norm minimization model, called TLNM for short, was proposed.

B. Optimization TLNM Algorithm Based on ADMM

Based on the augmented Lagrange formulation, one can get the following optimization problem:

$$\begin{aligned} \text{Lag}(\mathcal{X}, \mathcal{P}, \{\mathcal{M}_n, \mathcal{Q}_n, L_n, R_n, D_n, \Phi_n\}_{n=1}^N) \\ = \sum_{n=1}^N \alpha_n \|D_n\|_{2,1} + \frac{\mu}{2} \|\mathbf{M}_{n(n)} - L_n D_n R_n + \frac{\Phi_n}{\mu}\|_F^2 \\ + \frac{\mu}{2} \|\mathcal{M}_n - \mathcal{X} + \frac{\mathcal{Q}_n}{\mu}\|_F^2 + \frac{\mu}{2} \|\mathcal{X}_\Omega - \mathcal{T}_\Omega + \frac{\mathcal{P}_\Omega}{\mu}\|_F^2. \end{aligned} \quad (32)$$

where \mathcal{P} , \mathcal{Q}_n and Φ_n are the Lagrange multipliers and μ is a positive scalar. Now, we can optimize the problem (32) under the ADMM framework. Suppose that $L_n^k, R_n^k, D_n^k, \mathcal{M}_n^k, \mathcal{X}^k$ denote the result of the k th iteration in the ADMM.

1) *Optimizing $\{L_1, \dots, L_N\}$* : The initial value of L_n, D_n, R_n is $L_n^0 = eye(I_n, r_n)$, $D_n^0 = eye(r_n, r_n)$ and $R_n^0 = eye(r, t_n)$ and $t_n = I_1 \cdots I_{n-1} I_{n+1} \cdots I_N$. Keeping other variables constant, the optimization function with respect to L_n is

$$\min_{L_n, R_n^k} \|\mathbf{M}_{n(n)}^k - L_n D_n^k R_n^k + \frac{\Phi_n^k}{\mu}\|_F^2. \quad (33)$$

In our method, problem (33) is regarded as an iteration of CSVD-QR on $\mathbf{M}_{n(n)}^k + \frac{\Phi_n^k}{\mu}$, and its form is as follows:

$$\mathbf{M}_{n(n)}^k + \frac{\Phi_n^k}{\mu} = L_n D_{Tn} R_n^k, \quad (34)$$

where $D_{Tn} \in \mathbb{R}^{r_n \times r_n}$. Let $\mathbf{M}_{n(n)}^k + \frac{\Phi_n^k}{\mu} = G_n$. Then L_n^{k+1} can be updated as follows:

$$[Q, T] = qr(G_n R_n^{T(k)}) \quad (35)$$

$$L_n^{k+1} = Q(q_1, \dots, q_{r_n}) \quad (36)$$

where $Q \in \mathbb{R}^{I_n \times I_n}$ and $T \in \mathbb{R}^{I_n \times r_n}$ are the intermediate variables.

2) *Optimizing $\{R_1, \dots, R_N\}$* : Similarly, R_n^{k+1} can be updated as follows:

$$[Q, T] = qr(G_n^T L_n^{k+1}) \quad (37)$$

$$R_n^{k+1} = Q(q_1, \dots, q_{r_n}) \quad (38)$$

where $Q \in \mathbb{R}^{t_n \times t_n}$ and $T \in \mathbb{R}^{I_n \times r_n}$ are the intermediate variables. Since the optimal R_n is a row orthogonal matrix, we set

$$R_n^{k+1} = R_n^{T(k+1)} \quad (39)$$

3) *Optimizing $\{D_1, \dots, D_N\}$* : The variable D_n can be optimized, with $\mathbf{M}_{n(n)}^k, \Phi_n^k, L_n^{k+1}$, and R_n^{k+1} held fixed, by solving the following problem:

$$D_n^{k+1} = \arg \min_{D_n} \frac{\alpha_n}{\mu^k} \|D_n\|_{2,1} + \frac{1}{2} \|D_n - L_n^{T(k+1)} (\mathbf{M}_{n(n)}^{k+1} + \frac{\Phi_n^k}{\mu^k}) R_n^{T(k+1)}\|_F^2. \quad (40)$$

From (34) and (40), we have the conclusion:

$$D_{Tn} = L_n^{T(k+1)} (\mathbf{M}_{n(n)}^{k+1} + \frac{\Phi_n^k}{\mu^k}) R_n^{T(k+1)} \quad (41)$$

Therefore, (40) can be reformulated as follows:

$$D_n^{k+1} = \arg \min_{D_n} \frac{\alpha_n}{\mu^k} \|D_n\|_{2,1} + \frac{1}{2} \|D_n - D_{Tn}\|_F^2. \quad (42)$$

From Lemma 3, we can now update D_n by the following equation:

$$D_n^{k+1} = D_{Tn} K_n \quad (43)$$

where K_n is a diagonal matrix, i.e.,

$$K_n = \text{diag}(k_{n1}, \dots, k_{nr_n}) \quad (44)$$

where the j th entry k_{nj} is given as follows:

$$k_{nj} = \frac{\max\{\|D_{Tn}(:, j)\|_F - \frac{1}{\mu^k}, 0\}}{\|D_{Tn}(:, j)\|_F} \quad (45)$$

4) *Optimizing $\{\mathcal{M}_1, \dots, \mathcal{M}_N\}$* : Keeping other variables constant, the optimization function with respect to \mathcal{M}_n is

$$\mathcal{M}_n = \min_{\mathcal{M}_n} \|\mathbf{M}_{n(n)} - L_n^{k+1} D_n^{k+1} R_n^{k+1} + \frac{\Phi_n^k}{\mu^k}\|_F^2 + \|\mathcal{M}_n - \mathcal{X}^k + \frac{\mathcal{Q}_n^k}{\mu^k}\|_F^2. \quad (46)$$

By the definition of tensor Frobenius norm and matrix Frobenius norm, we equivalently reformulate \mathcal{M}_n of (46) as

$$\mathbf{M}_{n(n)} = \min_{\mathcal{M}_n} \|\mathbf{M}_{n(n)} - L_n^{k+1} D_n^{k+1} R_n^{k+1} + \frac{\Phi_n^k}{\mu^k}\|_F^2 + \|\mathbf{M}_{n(n)} - \mathbf{X}_{(n)}^k + \frac{\mathbf{Q}_{n(n)}^k}{\mu}\|_F^2. \quad (47)$$

Therefore $\mathbf{M}_{n(n)}^{k+1}$ is updated as follows:

$$\mathbf{M}_{n(n)}^{k+1} = \frac{1}{2} (\mathbf{X}_{(n)}^k - \frac{\mathbf{Q}_{n(n)}^k}{\mu^k} + L_n^{k+1} D_n^{k+1} R_n^{k+1} - \frac{\Phi_n^k}{\mu^k}). \quad (48)$$

Finally, the tensor \mathcal{M}_n is obtained by folding the matrix $\mathbf{M}_{n(n)}$. That is,

$$\mathcal{M}_n^{k+1} = \text{fold}_n(\mathbf{M}_{n(n)}^{k+1}). \quad (49)$$

5) *Optimizing \mathcal{X}* : We optimize the variable \mathcal{X} as follows:

$$\mathcal{X}^{k+1} = \min_{\mathcal{X}} \sum_{n=1}^N \frac{\mu}{2} \|\mathcal{M}_n^{k+1} - \mathcal{X} + \frac{\mathcal{Q}_n^k}{\mu^k}\|_F^2 + \frac{\mu}{2} \|\mathcal{X}_{\Omega} - \mathcal{T}_{\Omega} + \frac{\mathcal{P}_{\Omega}^k}{\mu^k}\|_F^2 \quad (50)$$

Its closed-form solution is

$$\begin{cases} \mathcal{X}_{\Omega} &= \frac{1}{(N+1)\mu^k} (\mathcal{S} + \mu^k \mathcal{T} - \mathcal{P}^k)_{\Omega}, \\ \mathcal{X}_{\Omega^{\perp}} &= \frac{1}{N\mu^k} (\mathcal{S})_{\Omega^{\perp}}, \end{cases} \quad (51)$$

where $\mathcal{S} = \sum_{n=1}^N \mu^k \mathcal{M}_n^{k+1} + \mathcal{Q}_n^k$, and Ω^{\perp} is the complement set of Ω .

6) *Updating the multipliers \mathcal{Q}_n, Φ_n and \mathcal{P}* :

$$\begin{cases} \mathcal{Q}_n^{k+1} &= \mathcal{Q}_n^k + \mu^k (\mathcal{M}_n^{k+1} - \mathcal{X}^{k+1}), \\ \Phi_n^{k+1} &= \Phi_n^k + \mu^k (\mathbf{M}_{n(n)}^{k+1} - L_n^{k+1} D_n^{k+1} R_n^{k+1}), \\ \mathcal{P}^{k+1} &= \mathcal{P}^k + \mu^k (\mathcal{X}_{\Omega} - \mathcal{T}_{\Omega}), \\ \mu^{k+1} &= \rho \mu^k, \end{cases} \quad (52)$$

where $\rho \geq 1$. The pseudo-code of our algorithm for TLNM is summarized in Algorithm 1.

C. Tensor $L_{2,1}$ -Norm Minimization with Total variation (TLNMTV)

It is well known that TV makes some details of the image better retained by improving the utilization rate of the local prior information of the image. Therefore, reasonable addition of regularization term of TV can further improve the accuracy of the model. In view of this, we propose the tensor $L_{2,1}$ norm minimization with TV (TLNMTV) method to obtain the following model by adding the regularization term of the form in [25].

$$\begin{aligned} \min_{\mathcal{X}} \quad & \sum_{n=1}^N \alpha_n \|\mathbf{X}_{(n)}\|_* + \lambda \sum_{n=1}^N \beta_n \|F_n \mathbf{X}_{(n)}\| \\ \text{s.t.} \quad & \mathcal{X}_{\Omega} = \mathcal{T}_{\Omega} \end{aligned} \quad (53)$$

Algorithm 1 TLNM

Input: an incomplete tensor \mathcal{T} , the index set of the known elements Ω , convergence criteria ϵ , maximum iteration number K .

Initialization: $\mathcal{X}^0 = \mathcal{T}_\Omega$, $\{\mathcal{M}_n^0 = \mathcal{X}^0\}_{n=1}^N$, $\mu^0 > 0$, $\rho > 1$, $\{\alpha_n, r_n, L_n^0, D_n^0, R_n^0\}_{n=1}^N$.

```

1: while not converged and  $k < K$  do
2:   for  $n=1:N$  do
3:     Updating  $L_n^k$  via (35-36);
4:     Updating  $R_n^k$  via (37-39);
5:     Updating  $D_n^k$  via (43);
6:     Updating  $\mathcal{M}_n^k$  via (48-49);
7:   end for
8:   Updating  $\mathcal{X}^k$  via (51);
9:   Updating the multipliers  $\mathcal{Q}_n^k$ ,  $\Phi_n^k$  and  $\mathcal{P}^k$  via (52);
10:   $\mu^k = \rho\mu^{k-1}$ ,  $k = k + 1$ ;
11:  Check the convergence conditions  $\|\mathcal{X}^{k+1} - \mathcal{X}^k\|_\infty \leq \epsilon$ 
12: end while
13: return  $\mathcal{X}^{k+1}$ 

```

Output: Completed tensor $\mathcal{X} = \mathcal{X}^{k+1}$

where the second term is the TV regularization term; the dimension of F_n is $(I_n - 1, I_n)$, where $(F_n)_{i,i} = 1$, $(F_n)_{i,i+1} = -1$; the operator $|\cdot|$, defined as $|X| = \sum_{i=1} \sum_{j=1} |X_{i,j}|$. λ is a tunable parameter; β_1, \dots, β_N is 0 or 1, which indicates whether we have a smooth and piecewise prior on the n -th mode of completed tensor. As we all know, different dimensions of different data represent different data information, and some of the information is not so smooth, so there is no need to calculate the smooth and piecewise prior information on this dimension. Thus, the use of TV regularization term is more reasonable (the TV term adopted here is just able to determine whether the smoothing and piecewise priors need to be calculated for different modes). In particular, when the TV regularization term is removed, this problem will degenerate into low-rank tensor problem (2). Similarly, we introduce the set of matrices $\{\mathcal{Q}_n\}_{n=1}^N$ and $\{\mathcal{A}_n\}_{n=1}^N$ and the set of tensors $\{\mathcal{Z}_n\}_{n=1}^N$ as auxiliary variables, where $\mathcal{A}_n = \mathbf{X}_{(n)}$, $\mathcal{Q}_n = F_n \mathcal{A}_n$ and $\mathcal{Z}_n = \mathcal{X}$. By taking advantage of the whole ideological process of the TLNN method, the proposed Tensor $L_{2,1}$ -norm Minimization with TV model can be obtained as follows:

$$\begin{aligned}
& \min_{\mathcal{X}} \sum_{n=1}^N \alpha_n \|\mathcal{D}_n\|_{2,1} + \lambda \sum_{n=1}^N \beta_n |\mathcal{Q}_n| \\
& s.t. \{ \mathcal{Z}_n = \mathcal{X} \}_{n=1}^N, \mathcal{X}_\Omega = \mathcal{T}_\Omega \\
& \quad \{ \mathcal{Q}_n = F_n \mathcal{A}_n, \mathcal{Z}_n = \mathcal{X}, \mathcal{A}_n = \mathbf{X}_{(n)} \}_{n=1}^N \\
& \quad \{ \mathcal{Z}_{n(n)} = L_n D_n R_n \}_{n=1}^N, \\
& \quad L_n^T L_n = I_n, R_n R_n^T = I_n.
\end{aligned} \tag{54}$$

Because of the convexity of the model (54), the ADMM technology can be used to solve such problem directly.

D. Optimization TLNMTV Algorithm Based on ADMM

By using the augmented Lagrange formulation, the optimization problem (54) is changed into:

$$Lag(\mathcal{X}, \mathcal{P}, \{\mathcal{Z}_n, \mathcal{G}_n, \mathcal{Q}_n, \Lambda_n, \mathcal{A}_n, \Gamma_n, L_n, R_n, D_n, \Phi_n\}_{n=1}^N)$$

$$\begin{aligned}
& = \sum_{n=1}^N (\alpha_n \|\mathcal{D}_n\|_{2,1} + \frac{\mu_1}{2} \|\mathcal{Z}_n - \mathcal{X} + \frac{\mathcal{G}_n}{\mu_1}\|_F^2) \\
& + \sum_{n=1}^N \beta_n (\lambda |\mathcal{Q}_n| + \frac{\mu_2}{2} \|\mathcal{Q}_n - F_n \mathcal{A}_n + \frac{\Lambda_n}{\mu_2}\|_F^2) \\
& + \sum_{n=1}^N \beta_n (\frac{\mu_3}{2} \|\mathcal{A}_n - \mathbf{X}_{(n)} + \frac{\Gamma_n}{\mu_3}\|_F^2) \\
& + \frac{\mu_4}{2} \|\mathcal{X}_\Omega - \mathcal{T}_\Omega + \frac{\mathcal{P}_\Omega}{\mu_4}\|_F^2 \\
& + \sum_{n=1}^N \frac{\mu_5}{2} \|\mathcal{Z}_{n(n)} - L_n D_n R_n + \frac{\Phi_n}{\mu_5}\|_F^2
\end{aligned} \tag{55}$$

where matrices $\{\Lambda_n\}_{n=1}^N$, $\{\Gamma_n\}_{n=1}^N$, $\{\Phi_n\}_{n=1}^N$ and tensors $\{\mathcal{G}_n\}_{n=1}^N$, \mathcal{P} are Lagrange multipliers, $\{\mu_i\}_{i=1}^5 > 0$. Next, we derive the update formulate of $\{\mathcal{Q}_n\}_{n=1}^N$, $\{\mathcal{L}_n\}_{n=1}^N$, $\{\mathcal{R}_n\}_{n=1}^N$, $\{\mathcal{D}_n\}_{n=1}^N$, $\{\mathcal{Z}_n\}_{n=1}^N$, $\{\mathcal{A}_n\}_{n=1}^N$ and \mathcal{X} .

1) *Optimizing $\{\mathcal{Q}_1, \dots, \mathcal{Q}_N\}$:* By keeping other variables fixed, we rewrite the optimization problem of $\{\mathcal{Q}_1, \dots, \mathcal{Q}_N\}$ into the following form:

$$\min_{\{\mathcal{Q}_1, \dots, \mathcal{Q}_N\}} \sum_{n=1}^N \beta_n (\lambda |\mathcal{Q}_n| + \frac{\mu_2}{2} \|\mathcal{Q}_n - F_n \mathcal{A}_n^k + \frac{\Lambda_n^k}{\mu_2}\|_F^2) \tag{56}$$

As $\{\mathcal{Q}_1, \dots, \mathcal{Q}_N\}$ are independent in the optimization problem, we can easily derive the update formula of \mathcal{Q}_n as:

$$\mathcal{Q}_n = \beta_n \cdot shrinkage_{\frac{\lambda}{\mu_2}} (F_n \mathcal{A}_n^k - \frac{1}{\mu_2} \Lambda_n^k) \tag{57}$$

where $shrinkage_\alpha(\cdot)$ is the elementwise shrinkage thresholding operator of a matrix, i.e.,

$$shrinkage_\alpha(X)_{i,j} = (X)_{i,j} - \min(\alpha, |(X)_{i,j}|) \cdot \frac{(X)_{i,j}}{|(X)_{i,j}|}$$

and $\frac{(X)_{i,j}}{|(X)_{i,j}|}$ is defined as zero when $(X)_{i,j} = 0$.

2) *Optimizing $\{L_1, \dots, L_N\}$:* The initial value of L_n, D_n, R_n is $L_n^0 = eye(I_n, r_n)$, $D_n^0 = eye(r_n, r_n)$ and $R_n^0 = eye(r, t_n)$ and $t_n = I_1 \cdots I_{n-1} I_{n+1} \cdots I_N$. Keeping other variables constant, the optimization function with respect to L_n is

$$\min_{L_n, R_n^k} \|\mathcal{Z}_{n(n)}^k - L_n D_n^k R_n^k + \frac{\Phi_n^k}{\mu_5}\|_F^2. \tag{58}$$

Similarly, problem (58) is regarded as an iteration of CSVD-QR on $\mathcal{Z}_{n(n)}^k + \frac{\Phi_n^k}{\mu_5}$, and its form is as follows:

$$\mathcal{Z}_{n(n)}^k + \frac{\Phi_n^k}{\mu_5} = L_n D_{Tn} R_n^k, \tag{59}$$

where $D_{Tn} \in \mathbb{R}^{r_n \times r_n}$. Let $\mathcal{Z}_{n(n)}^k + \frac{\Phi_n^k}{\mu_5} = B_n$. Then L_n^{k+1} can be updated as follows:

$$[E, T] = qr(B_n R_n^{T(k)}) \tag{60}$$

$$L_n^{k+1} = E(q_1, \dots, q_{r_n}) \tag{61}$$

where $E \in \mathbb{R}^{I_n \times I_n}$ and $T \in \mathbb{R}^{I_n \times r_n}$ are the intermediate variables.

3) *Optimizing $\{R_1, \dots, R_N\}$* : Similarly, R_n^{k+1} can be updated as follows:

$$[E, T] = qr(B_n^T L_n^{k+1}) \quad (62)$$

$$R_n^{k+1} = E(q_1, \dots, q_{r_n}) \quad (63)$$

where $E \in \mathbb{R}^{t_n \times t_n}$ and $T \in \mathbb{R}^{t_n \times r_n}$ are the intermediate variables. Since the optimal R_n is a row orthogonal matrix, we set

$$R_n^{k+1} = R_n^{T(k+1)} \quad (64)$$

4) *Optimizing $\{D_1, \dots, D_N\}$* : The variable D_n can be optimized, with $\mathbf{Z}_{n(n)}^k$, Φ_n^k , L_n^{k+1} , and R_n^{k+1} held fixed, by solving the following problem:

$$D_n^{k+1} = \arg \min_{D_n} \frac{\alpha_n}{\mu_5^k} \|D_n\|_{2,1} + \frac{1}{2} \|D_n - L_n^{T(k+1)} (\mathbf{Z}_{n(n)}^{k+1} + \frac{\Phi_n^k}{\mu_5^k}) R_n^{T(k+1)}\|_F^2. \quad (65)$$

From (59) and (65), we have the following conclusion:

$$D_{Tn} = L_n^{T(k+1)} (\mathbf{Z}_{n(n)}^{k+1} + \frac{\Phi_n^k}{\mu_5^k}) R_n^{T(k+1)} \quad (66)$$

Therefore, (65) can be reformulated as follows:

$$D_n^{k+1} = \arg \min_{D_n} \frac{\alpha_n}{\mu_5^k} \|D_n\|_{2,1} + \frac{1}{2} \|D_n - D_{Tn}\|_F^2. \quad (67)$$

From Lemma 3, the minimization problem in (67) can be solved by the LNMS as follows:

$$D_n^{k+1} = D_{Tn} K_n \quad (68)$$

where K_n is a diagonal matrix, i.e.,

$$K_n = \text{diag}(k_{n1}, \dots, k_{nr_n}) \quad (69)$$

where the j th entry k_{nj} can be given as follows:

$$k_{nj} = \frac{\max\{\|D_{Tn}(:, j)\|_F - \frac{1}{\mu_5^k}, 0\}}{\|D_{Tn}(:, j)\|_F} \quad (70)$$

5) *Optimizing $\{\mathbf{Z}_1, \dots, \mathbf{Z}_N\}$* : Keeping other variables constant, the optimization function with respect to \mathbf{Z}_n is

$$\mathbf{Z}_n = \min_{\mathbf{Z}_n} \frac{\mu_5^k}{2} \|\mathbf{Z}_{n(n)} - L_n^{k+1} D_n^{k+1} R_n^{k+1} + \frac{\Phi_n^k}{\mu_5^k}\|_F^2 + \frac{\mu_1^k}{2} \|\mathbf{Z}_n - \mathcal{X}^k + \frac{\mathbf{Q}_n^k}{\mu_1}\|_F^2. \quad (71)$$

By the definition of tensor Frobenius norm and matrix Frobenius norm, we equivalently reformulate \mathbf{Z}_n of (71) as

$$\mathbf{Z}_{n(n)} = \min_{\mathbf{Z}_n} \frac{\mu_5^k}{2} \|\mathbf{Z}_{n(n)} - L_n^{k+1} D_n^{k+1} R_n^{k+1} + \frac{\Phi_n^k}{\mu_5^k}\|_F^2 + \frac{\mu_1^k}{2} \|\mathbf{Z}_{n(n)} - \mathbf{X}_{(n)} + \frac{\mathbf{Q}_{n(n)}}{\mu_1}\|_F^2. \quad (72)$$

Therefore $\mathbf{Z}_{n(n)}^{k+1}$ is updated as follows:

$$\mathbf{Z}_{n(n)}^{k+1} = \frac{1}{\mu_1^k + \mu_5^k} (\mu_1^k \mathbf{X}_{(n)}^k - \mathbf{Q}_{n(n)}^k + \mu_5^k L_n^{k+1} D_n^{k+1} R_n^{k+1} - \Phi_n^k). \quad (73)$$

Finally, because we need to get the tensor \mathbf{Z}_n , we need to fold the matrix $\mathbf{Z}_{n(n)}$. So \mathbf{Z}_n is obtained by the following equation:

$$\mathbf{Z}_n = \text{fold}_n(\mathbf{Z}_{n(n)}). \quad (74)$$

Algorithm 2 TLNMTV

Input: an incomplete tensor \mathcal{T} , the index set of the known elements Ω , convergence criteria ϵ , maximum iteration number K .

Initialization: $\mathcal{X}^0 = \mathcal{T}_\Omega$, $\{\mathbf{Z}_n^0 = \mathcal{X}^0\}_{n=1}^N$, $\{\mu_i^0\}_{i=1}^5 > 0$, $\rho > 1$, $\{\alpha_n, r_n, L_n^0, D_n^0, R_n^0\}_{n=1}^N$.

```

1: while not converged and  $k < K$  do
2:   for  $n=1:N$  do
3:     Updating  $\mathbf{Q}_n^k$  via (57);
4:     Updating  $L_n^k$  via (60-61);
5:     Updating  $R_n^k$  via (62-64);
6:     Updating  $D_n^k$  via (68);
7:     Updating  $\mathbf{Z}_n^k$  via (73-74);
8:     Updating  $A_n^k$  via (77);
9:   end for
10:  Updating  $\mathcal{X}^k$  via (79-80);
11:  Updating the multipliers  $\mathcal{G}_n$ ,  $\Lambda_n$ ,  $\Phi_n$ ,  $\Gamma_n$ , and  $\mathcal{P}$  via (81);
12:   $\mu_1^{k+1} = \rho \mu_1^k$ ,  $\mu_2^{k+1} = \rho \mu_2^k$ ,  $\mu_3^{k+1} = \rho \mu_3^k$ ,
13:   $\mu_4^{k+1} = \rho \mu_4^k$ ,  $\mu_5^{k+1} = \rho \mu_5^k$ ,  $k = k + 1$ ;
14:  Check the convergence conditions  $\|\mathcal{X}^{k+1} - \mathcal{X}^k\|_\infty \leq \epsilon$ 
15: end while
16: return  $\mathcal{X}^{k+1}$ 

```

Output: Completed tensor $\mathcal{X} = \mathcal{X}^{k+1}$

6) *Optimizing $\{A_1, \dots, A_N\}$* : By keeping other variables fixed, we rewrite the optimization problem of $\{A_1, \dots, A_N\}$ into the following form:

$$\min_{\{A_1, \dots, A_N\}} \sum_{n=1}^N \beta_n \left(\frac{\mu_2^k}{2} \|\mathbf{Q}_n^{k+1} - F_n A_n + \frac{\Lambda_n^k}{\mu_2^k}\|_F^2 \right) + \sum_{n=1}^N \beta_n \left(\frac{\mu_3^k}{2} \|A_n - \mathbf{X}_{(n)}^k + \frac{\Gamma_n^k}{\mu_3^k}\|_F^2 \right) \quad (75)$$

(75) can be decomposed into N sub-problems to solve. Then the sub-problem can be expressed as the following form:

$$A_n^{k+1} = \arg \min_{A_n} \beta_n \left(\frac{\mu_2^k}{2} \|\mathbf{Q}_n^k - F_n A_n + \frac{\Lambda_n^k}{\mu_2^k}\|_F^2 \right) + \beta_n \left(\frac{\mu_3^k}{2} \|A_n - \mathbf{X}_{(n)}^k + \frac{\Gamma_n^k}{\mu_3^k}\|_F^2 \right) \quad (76)$$

Hence, the following update formula is deduced by solving the minimization problem:

$$A_n^{k+1} = \beta_n (\mu_2^k F_n^T F_n + \mu_3^k I)^{-1} (F_n^T \Lambda_n^k + \mu_2^k F_n^T \mathbf{Q}_n^{k+1} + \mu_3^k \mathbf{X}_{(n)}^k - \Gamma_n^k) \quad (77)$$

where I is the identify matrix.

7) *Optimizing \mathcal{X}* : We optimize the variable \mathcal{X} as follows:

$$\mathcal{X}^{k+1} = \min_{\mathcal{X}} \sum_{n=1}^N \left(\frac{\mu_1^k}{2} \|\mathbf{Z}_n^{k+1} - \mathcal{X} + \frac{\mathcal{G}_n^k}{\mu_1^k}\|_F^2 \right) + \sum_{n=1}^N \beta_n \left(\frac{\mu_3^k}{2} \|A_n^{k+1} - \mathbf{X}_{(n)} + \frac{\Gamma_n^k}{\mu_3^k}\|_F^2 \right) + \frac{\mu_4^k}{2} \|\mathcal{X}_\Omega - \mathcal{T}_\Omega + \frac{\mathcal{P}_\Omega}{\mu_4^k}\|_F^2 \quad (78)$$

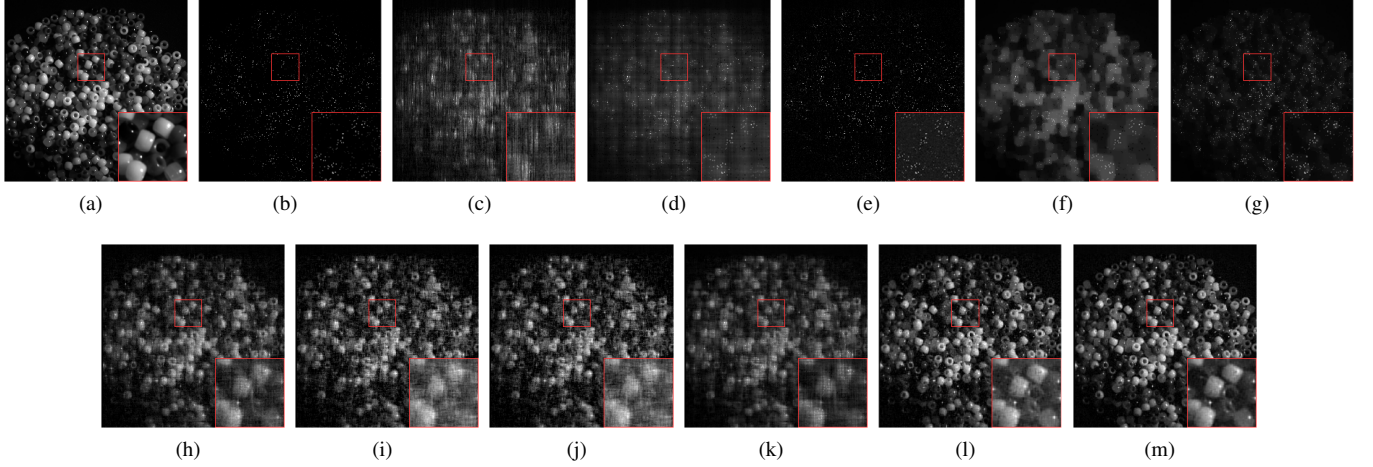


Fig. 1. (a) Original images 27-th slice of beads. (b) Corresponding sampled images with SR 5%. (c)-(l) and (m) Completed images achieved by nine competing methods and proposed TLNM method and TLNMTV method, respectively. (a) Original image. (b) Corrupted image. (c) MC-ALM. (d) HaLRTC. (e) TMac. (f) LRTC-TV. (g) Trace/TV. (h) t-SVD. (i) McpTC. (j) ScadTC. (k) FTNN. (l) TLNM. (m) TLNMTV.

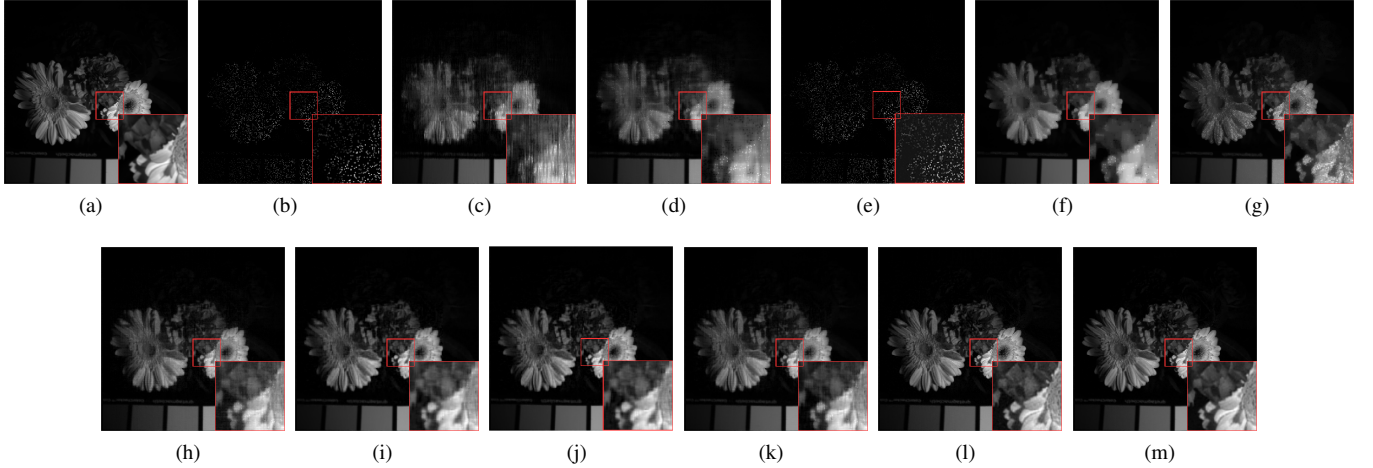


Fig. 2. (a) Original images 22-th slice of flowers. (b) Corresponding sampled images with SR 10%. (c)-(l) and (m) Completed images achieved by nine competing methods and proposed TLNM method and TLNMTV method, respectively. (a) Original image. (b) Corrupted image. (c) MC-ALM. (d) HaLRTC. (e) TMac. (f) LRTC-TV. (g) Trace/TV. (h) t-SVD. (i) McpTC. (j) ScadTC. (k) FTNN. (l) TLNM. (m) TLNMTV.

Its closed-form solution is

$$X_{\Omega} = \frac{[S_1 + \mu_4^k \mathcal{T} - \mathcal{P}^k + S_2]_{\Omega}}{N\mu_1^k + \sum_{n=1}^N \beta_n \mu_3^k + \mu_4}, \quad (79)$$

$$X_{\Omega^{\perp}} = \frac{[S_1 + S_2]_{\Omega^{\perp}}}{N\mu_1^k + \sum_{n=1}^N \beta_n \mu_3^k}, \quad (80)$$

where $S_1 = \sum_{n=1}^N \mu_1^k \mathcal{Z}_n^{k+1} + \mathcal{G}_n^k$, $S_2 = \sum_{n=1}^N fold_n(\mu_3^k A_n^{k+1} + \Gamma_n^k)$ and Ω^{\perp} is the complement set of Ω .

8) *Updating the multipliers \mathcal{G}_n , Λ_n , Φ_n , Γ_n , and \mathcal{P} :*

$$\begin{cases} \mathcal{G}_n^{k+1} = \mathcal{G}_n^k + \mu_1^k (\mathcal{Z}_n^{k+1} - X^{k+1}), \\ \Lambda_n^{k+1} = \Lambda_n^k + \mu_2 (\mathcal{Q}_n^{k+1} - F_n A_n^{k+1}), \\ \Gamma_n^{k+1} = \Gamma_n^k + \mu_3 (A_n^{k+1} - \mathbf{X}_{(n)}^{k+1}), \\ \mathcal{P}^{k+1} = \mathcal{P}^k + \mu_4 (\mathcal{X}_{\Omega}^{k+1} - \mathcal{T}_{\Omega}), \\ \Phi_n^{k+1} = \Phi_n^k + \mu_5 (\mathbf{Z}_{n(n)}^{k+1} - L_n^{k+1} D_n^{k+1} R_n^{k+1}), \end{cases} \quad (81)$$

and $\mu_1^{k+1} = \rho \mu_1^k$, $\mu_2^{k+1} = \rho \mu_2^k$, $\mu_3^{k+1} = \rho \mu_3^k$, $\mu_4^{k+1} = \rho \mu_4^k$, $\mu_5^{k+1} = \rho \mu_5^k$, where $\rho \geq 1$. The pseudo-code of our algorithm for TLNMTV is summarized in Algorithm 2.

E. Computational Complexity Analysis

For an N th-order input tensor $\mathcal{T} \in \mathbb{R}^{I_1 \times I_2 \times \dots \times I_N}$ the computational complexity of Algorithm 1 is mainly composed of the following five parts.

1) : Updating L_n needs to perform QR decomposition [see (35)-(36)], its complexity is $O(I_n r_n^2)$, and the complexity of variables $L_n (n = 1, 2, \dots, N)$ is $O(\sum_{n=1}^N I_n r_n^2)$.

2) : Similarly, the complexity of updating R_n is $O(\sum_{n=1}^N r_n^2 \prod_{i=1, i \neq n}^N I_i)$.

3) : Updating D_n needs to perform LNMS on a matrix of $r_n \times r_n$, the complexity of variables $D_n (n = 1, 2, \dots, N)$ is $O(\sum_{n=1}^N r_n^2)$.

4) : Updating \mathcal{M}_n needs to perform $L_n D_n R_n$, the complexity of variables $\mathcal{M}_n (n = 1, 2, \dots, N)$ is $O(\sum_{n=1}^N (I_n r_n^2 + r \prod_{i=1}^N I_i))$.

5) : The complexity of updating \mathcal{X} is $O(\prod_{i=1}^N I_i)$. Thus, the overall computational complexity of our Algorithm 1 is $O(K(\sum_{n=1}^N (I_n r_n^2 + r_n^2 \prod_{i=1, i \neq n}^N I_i + I_n r_n^2 + r \prod_{i=1}^N I_i) + \prod_{i=1}^N I_i))$.

TABLE I
AVERAGE QUANTITATIVE EVALUATION OF THE RESULTS FOR DIFFERENT HSIs WITH SRs 5%

HSI	index	MC-ALM	HaLRTC	TMac	LRTC-TV	Trace-TV	t-SVD	McpTC	ScadTC	FTNN	TLNM	TLNMTV
	PSNR	22.94	23.00	11.03	25.09	17.64	28.99	30.97	30.33	27.83	33.56	34.42
	SSIM	0.6813	0.7562	0.3009	0.8403	0.7446	0.8344	0.8778	0.8438	0.8573	0.8985	0.9288
	FSIM	0.8151	0.8432	0.6710	0.8856	0.8423	0.9282	0.9340	0.9187	0.9168	0.9608	0.9705
	ERGAS	294.46	290.15	1141.14	246.07	546.93	161.31	116.88	125.13	167.10	85.03	77.96
	TIME	13.21	53.60	9.16	665.53	133.78	2014.86	1353.69	1352.08	777.86	252.57	560.89
	PSNR	21.83	21.34	14.64	22.27	19.02	25.32	25.02	24.41	24.67	27.33	29.64
	SSIM	0.3714	0.4269	0.0661	0.4799	0.4457	0.6076	0.5423	0.4892	0.5808	0.6791	0.8078
	FSIM	0.7034	0.6319	0.6039	0.6553	0.6830	0.8622	0.8285	0.8348	0.8034	0.9057	0.9503
	ERGAS	349.15	366.77	772.13	318.40	481.15	224.22	239.92	256.12	247.09	178.22	135.08
	TIME	13.69	41.60	12.81	688.56	129.47	659.29	1358.84	1342.90	615.05	245.51	569.51
	PSNR	24.89	23.36	13.65	24.10	17.80	28.95	31.13	30.29	27.69	31.05	32.35
	SSIM	0.7458	0.7657	0.2382	0.8269	0.6720	0.8063	0.8615	0.8031	0.8626	0.7883	0.8357
	FSIM	0.8554	0.8489	0.6933	0.8621	0.8317	0.9225	0.9350	0.9172	0.9182	0.9322	0.9518
	ERGAS	266.39	316.31	961.35	291.41	601.18	170.27	129.79	142.29	195.04	131.49	115.39
	TIME	13.63	45.32	11.35	702.82	136.35	1759.81	1335.80	1329.24	708.78	256.42	593.73
	PSNR	27.03	27.19	16.82	28.91	20.89	30.93	33.91	34.49	32.17	36.21	38.08
	SSIM	0.7270	0.7813	0.4395	0.8469	0.7502	0.7943	0.8764	0.8817	0.8691	0.8790	0.9217
	FSIM	0.8597	0.8679	0.7418	0.8839	0.8551	0.9180	0.9360	0.9428	0.9307	0.9601	0.9759
	ERGAS	273.48	267.66	861.85	220.63	573.05	181.44	122.77	114.76	157.17	94.68	78.27
	TIME	13.93	44.25	20.50	731.70	138.79	2125.98	1467.32	1469.87	645.16	260.80	594.41
	PSNR	18.50	17.70	14.48	18.53	16.08	21.84	20.90	20.87	21.21	25.85	27.60
	SSIM	0.3452	0.4299	0.1510	0.5493	0.4897	0.5004	0.3492	0.3445	0.5668	0.6288	0.7530
	FSIM	0.7036	0.6277	0.5638	0.6582	0.6106	0.8292	0.7803	0.7797	0.8044	0.9005	0.9387
	ERGAS	565.89	619.59	886.97	564.03	746.56	383.04	429.07	430.70	417.67	243.53	199.10
	TIME	13.38	34.29	14.19	696.72	133.18	1001.65	1350.77	1301.45	531.56	263.70	562.80
	PSNR	25.43	25.38	14.65	26.66	20.52	30.05	30.50	30.98	29.86	32.82	33.89
	SSIM	0.6851	0.7419	0.1597	0.7121	0.6263	0.8207	0.8409	0.8453	0.8410	0.8657	0.8979
	FSIM	0.8463	0.8421	0.6735	0.8336	0.8248	0.9293	0.9138	0.9229	0.9172	0.9558	0.9678
	ERGAS	244.26	244.85	813.44	210.52	423.86	141.91	135.26	128.21	147.41	102.12	90.54
	TIME	13.86	45.32	13.75	690.44	133.21	1781.95	1387.73	1385.49	494.37	256.82	566.00

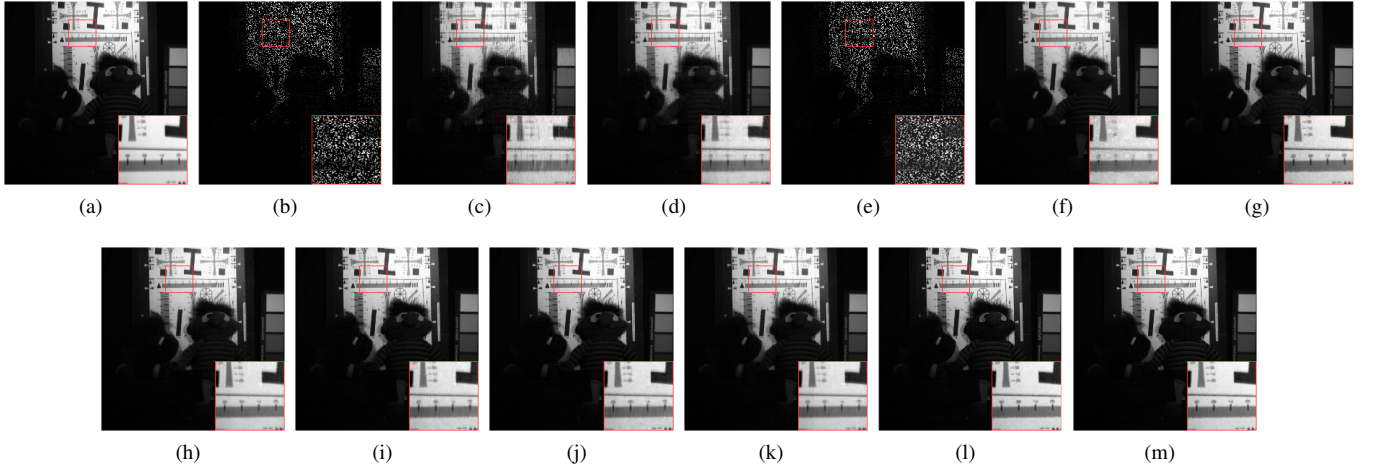


Fig. 3. (a) Original images 4-th slice of chart and stuffed toys. (b) Corresponding sampled images with SR 20%. (c)-(l) and (m) Completed images achieved by nine competing methods and proposed TLNM method and TLNMTV method, respectively. (a) Original image. (b) Corrupted image. (c) MC-ALM. (d) HaLRTC. (e) TMac. (f) LRTC-TV. (g) Trace/TV. (h) t-SVD. (i) McpTC. (j) ScadTC. (k) FTNN. (l) TLNM. (m) TLNMTV.

Similarly, the computational complexity of Algorithm 2 is mainly composed of the following seven parts.

6) : The complexity of updating \mathcal{Q}_n is $O(\sum_{n=1}^N (I_n - 1) \prod_n I_n)$.

7) : Updating L_n needs to perform QR decomposition [see (60)-(61)], its complexity is $O(I_n r_n^2)$, and the complexity of variables $L_n (n = 1, 2, \dots, N)$ is $O(\sum_{n=1}^N I_n r_n^2)$.

8) : Similarly, the complexity of updating R_n is $O(\sum_{n=1}^N r_n^2 \prod_{i=1, i \neq n}^N I_i)$.




9) : Updating D_n needs to perform LNMS on a matrix of $r_n \times r_n$, the complexity of variables $D_n (n = 1, 2, \dots, N)$ is $O(\sum_{n=1}^N r_n^2)$.

10) : Updating \mathcal{Z}_n needs to perform $L_n D_n R_n$, the complexity of variables $\mathcal{Z}_n (n = 1, 2, \dots, N)$ is $O(\sum_{n=1}^N (I_n r_n^2 + r \prod_{i=1}^N I_i))$.

11) : Updating A_n needs computing the inverse of a matrix of size $I_n \times I_n$ and matrix product, its complexity is $O(I_n^3 + I_n^2 \prod_{i=1, i \neq n}^N I_i)$. The complexity of variables $A_n (n = 1, 2, \dots, N)$ is $O(\sum_{n=1}^N I_n^3 + I_n^2 \prod_{i=1, i \neq n}^N I_i)$.

12) : The complexity of updating \mathcal{X} is $O(\prod_n I_n)$. Thus, the overall computational complexity of our Algorithm 2 is $O(K(\sum_{n=1}^N ((I_n - 1) \prod_n I_n + I_n r_n^2 + r_n^2 \prod_{i=1, i \neq n}^N I_i + r_n^2 + I_n r_n^2 + r \prod_{i=1}^N I_i + I_n^3 + I_n^2 \prod_{i=1, i \neq n}^N I_i) + \prod_n I_n))$.

TABLE II
AVERAGE QUANTITATIVE EVALUATION OF THE RESULTS FOR DIFFERENT HSI IS WITH SRs 10%

HSI	index	MC-ALM	HaLRTC	TMac	LRTC-TV	Trace-TV	t-SVD	McpTC	ScadTC	FTNN	TLNM	TLNMTV
	PSNR	26.16	27.46	11.29	28.72	29.79	33.01	34.19	34.44	32.89	36.42	37.66
	SSIM	0.7834	0.8558	0.3581	0.9122	0.9109	0.9097	0.9366	0.9346	0.9354	0.9384	0.9586
	FSIM	0.8826	0.9126	0.6937	0.9443	0.9625	0.9654	0.9668	0.9666	0.9688	0.9804	0.9869
	ERGAS	203.51	173.71	1107.83	162.84	137.79	104.12	80.64	78.36	93.19	62.34	53.94
	TIME	13.46	39.93	10.79	650.09	138.03	2002.84	1376.63	1377.41	551.72	279.96	575.33
	PSNR	23.31	23.23	14.88	24.74	24.88	28.86	27.15	25.95	28.06	29.80	33.77
	SSIM	0.4837	0.5278	0.0895	0.6250	0.7119	0.7823	0.6753	0.6076	0.7685	0.7892	0.9109
	FSIM	0.7761	0.7376	0.6578	0.7935	0.8829	0.9361	0.8997	0.8805	0.9144	0.9456	0.9800
	ERGAS	293.88	295.26	751.11	240.52	241.44	148.11	185.60	212.38	165.51	132.98	85.12
	TIME	13.21	29.55	17.67	676.59	135.13	757.86	1356.03	1354.90	448.22	276.19	618.32
	PSNR	27.77	27.43	13.97	28.90	25.28	32.81	34.57	34.44	32.77	32.86	34.15
	SSIM	0.8350	0.8558	0.3027	0.9078	0.8226	0.8929	0.9283	0.9181	0.9342	0.8291	0.8696
	FSIM	0.9129	0.9113	0.7167	0.9372	0.9355	0.9603	0.9664	0.9637	0.9674	0.9541	0.9677
	ERGAS	191.43	198.22	925.86	169.19	265.03	112.08	87.46	88.80	109.49	111.22	99.00
	TIME	13.29	39.21	17.48	693.80	142.60	1964.98	1414.35	1418.80	557.74	281.91	615.03
	PSNR	30.12	31.09	17.06	33.28	29.57	34.90	37.59	37.99	36.77	39.61	41.27
	SSIM	0.8141	0.8632	0.4777	0.9202	0.8832	0.8846	0.9355	0.9393	0.9375	0.9268	0.9531
	FSIM	0.9099	0.9213	0.7671	0.9439	0.9531	0.9557	0.9686	0.9711	0.9706	0.9821	0.9892
	ERGAS	193.02	170.17	838.63	131.55	236.64	116.67	79.59	75.70	90.55	69.00	59.37
	TIME	13.78	40.08	47.05	711.11	143.94	2144.85	1583.31	1613.61	514.21	322.76	686.35
	PSNR	20.50	20.14	14.75	22.39	20.93	25.37	24.91	24.89	25.50	28.72	30.29
	SSIM	0.4722	0.5456	0.1703	0.7602	0.7385	0.6783	0.5710	0.5673	0.7654	0.7508	0.8282
	FSIM	0.7879	0.7577	0.6356	0.8447	0.8440	0.9106	0.8700	0.8698	0.9177	0.9482	0.9659
	ERGAS	449.21	468.17	860.07	369.15	443.70	256.98	275.30	276.04	254.95	176.43	148.27
	TIME	13.47	35.46	48.30	692.61	138.45	1026.51	1459.46	1376.60	497.27	297.65	655.37
	PSNR	28.00	28.47	14.96	29.37	29.03	33.30	33.20	33.58	33.70	35.32	36.65
	SSIM	0.7770	0.8227	0.2177	0.7794	0.8075	0.8951	0.8942	0.8977	0.9134	0.9112	0.9407
	FSIM	0.8941	0.8971	0.7046	0.9004	0.9379	0.9635	0.9513	0.9559	0.9639	0.9761	0.9834
	ERGAS	181.48	171.19	785.53	154.65	160.09	97.78	99.63	95.54	94.21	78.77	66.61
	TIME	13.36	35.13	21.90	678.16	138.61	2000.64	1396.37	1395.25	376.01	295.87	601.74

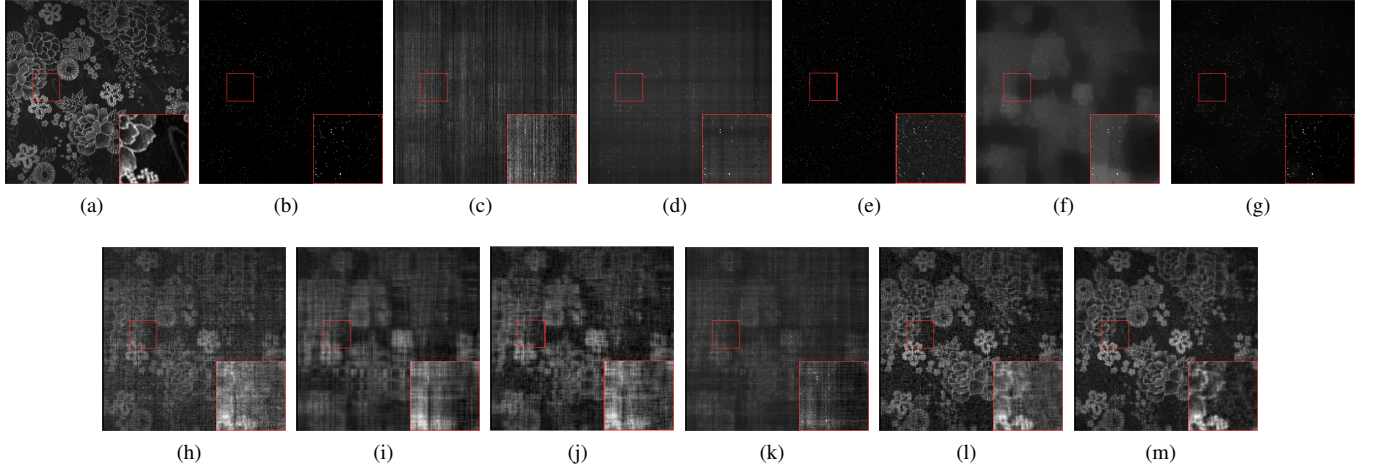


Fig. 4. (a) Original images 3-th slice of cloth. (b) Corresponding sampled images with SR 2.5%. (c)-(l) and (m) Completed images achieved by nine competing methods and proposed TLNM method and TLNMTV method, respectively. (a) Original image. (b) Corrupted image. (c) MC-ALM. (d) HaLRTC. (e) TMac. (f) LRTC-TV. (g) Trace-TV. (h) t-SVD. (i) McpTC. (j) ScadTC. (k) FTNN. (l) TLNM. (m) TLNMTV.

IV. EXPERIMENTS

In this section, three typical tensors data, i.e., HSI data, MRI data and color video data are employed to illustrate the performance of the proposed method. In addition to the time measurement (TIME for short) used to estimate the solution speed, four quantitative picture quality indices (PQIs) are also used to evaluate the quality of recovery, including peak signal-to-noise ratio (PSNR), structural similarity (SSIM) [30] feature similarity (FSIM) [31], and erreur relative globale adimensionnelle de synthèse (ERGAS) [32].

We compare our results with nine recently developed state-of-the-art LRTC methods, including the tensor trace

norm-based LRTC (HaLRTC) [18], the t-SVD-based TC method [33], ADMM(ALM)-based matrix completion (MC-ALM) [34], the nonconvex tensor rank constraint-based, i.e., the minimax concave plus penalty-based TC (McpTC) and the smoothly clipped absolute deviation penalty-based TC (ScadTC) method [35], the parallel matrix factorization-based LRTC method (TMac) [24], the LRTC with TV on tensor unfolding (LRTC-TV) [25], Tensor Completion based Framelet Representation of Tensor Nuclear Norm (FTNN) [36], and the joint trace/TV-based TC method (Trace-TV) [37].

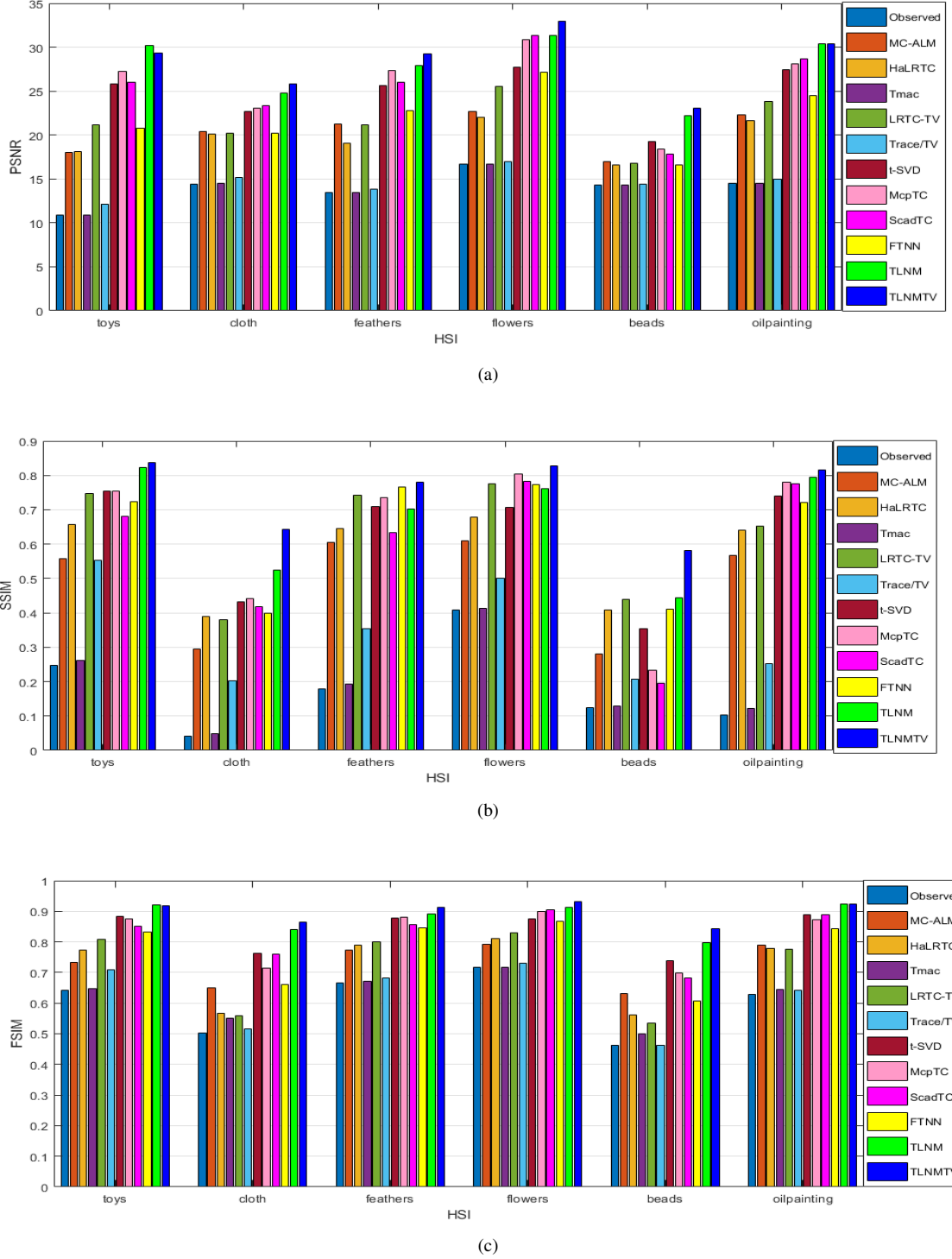


Fig. 5. The PSNR, SSIM, and FSIM of the results by different methods on all the HSI data with the sampling rate 2.5%.

A. HSI Completion

The HSI¹ test data use in the experiment came from the open source CAVE data sets. The size of HSI is $512 \times 512 \times 31$, indicating that the spatial resolution is 512×512 and the spectral resolution is 31, respectively. The main results at sampling rates of 5%, 10% and 20% are shown and reported

respectively in Figs. 1-3 and Tables I-II, from which it can be observed that our method can obtain better results under various SRs.

In detail, as one can see from the visuals in Figs. 1-3, the results of TMac are extremely unpleasant for all SR cases. Although the MC-ALM, HALRTC and Trace/TV methods are better than TMac in terms of recovery effect, the image effect obtained is far worse than the other methods. In addition, t-

¹<http://www.cs.columbia.edu/CAVE/databases/multispectral/>

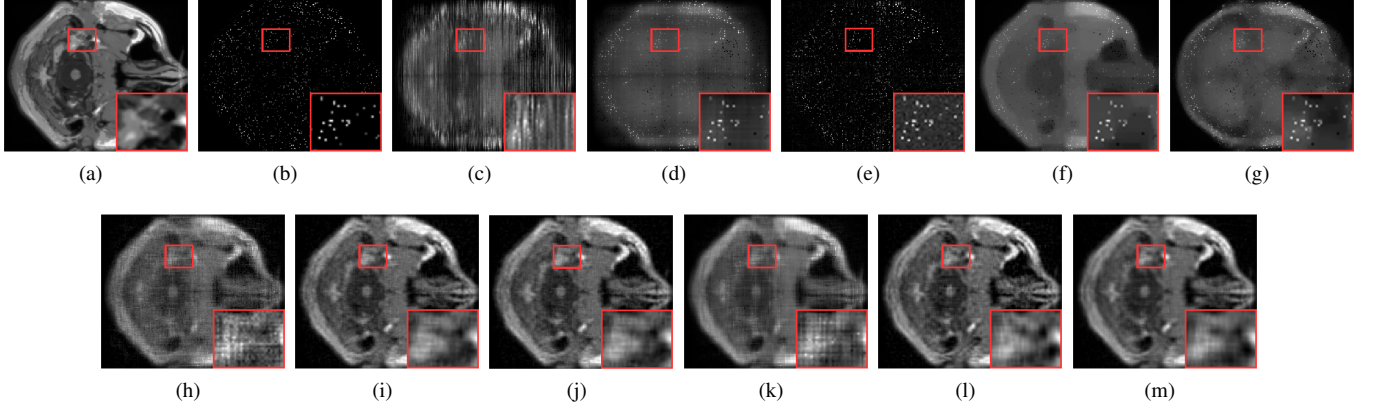


Fig. 6. (a) Original images 6-th slice of MRI. (b) Corresponding sampled images with SR 5%. (c)-(l) and (m) Completed images achieved by nine competing methods and proposed TLNM method and TLNMTV method, respectively. (a) Original image. (b) Corrupted image. (c) MC-ALM. (d) HaLRTC. (e) TMac. (f) LRTC-TV. (g) Trace/TV. (h) t-SVD. (i) McpTC. (j) ScadTC. (k) FTNN. (l) TLNM. (m) TLNMTV.

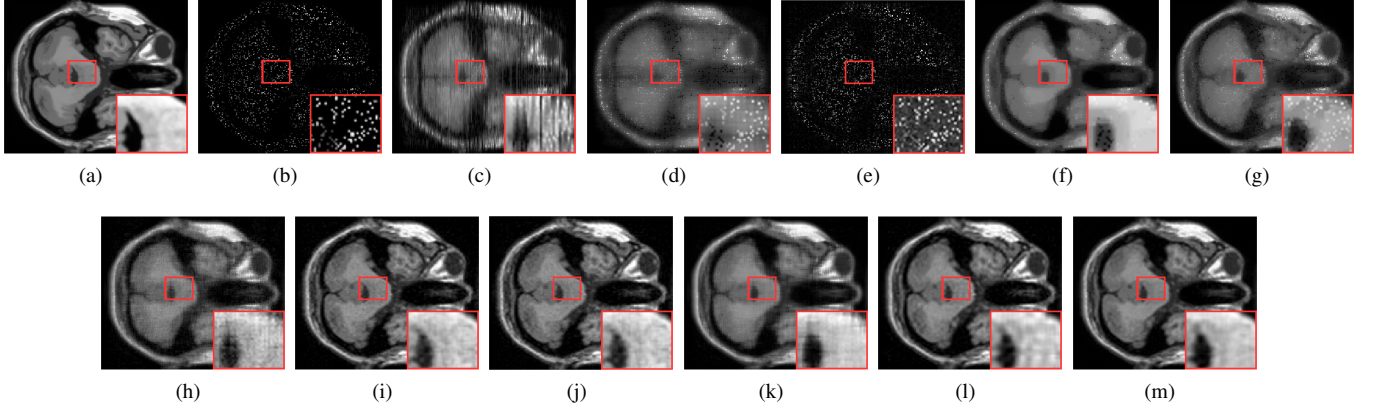


Fig. 7. (a) Original images 35-th slice of MRI. (b) Corresponding sampled images with SR 10%. (c)-(l) and (m) Completed images achieved by nine competing methods and proposed TLNM method and TLNMTV method, respectively. (a) Original image. (b) Corrupted image. (c) MC-ALM. (d) HaLRTC. (e) TMac. (f) LRTC-TV. (g) Trace/TV. (h) t-SVD. (i) McpTC. (j) ScadTC. (k) FTNN. (l) TLNM. (m) TLNMTV.

TABLE III
AVERAGE QUANTITATIVE EVALUATION OF THE RESULTS FOR MRI WITH DIFFERENT SRs

SR	index	Observed	MC-ALM	HaLRTC	TMac	LRTC-TV	Trace-TV	t-SVD	McpTC	ScadTC	FTNN	TLNM	TLNMTV
5%	PSNR	9.91	17.51	16.93	9.95	19.00	18.10	22.72	27.52	27.53	24.16	27.23	27.54
	SSIM	0.1740	0.2889	0.2987	0.1027	0.5297	0.4643	0.5136	0.7480	0.7483	0.6535	0.7237	0.7816
	FSIM	0.4573	0.6696	0.6144	0.5534	0.6629	0.6570	0.7705	0.8552	0.8553	0.8195	0.8453	0.8566
	ERGAS	1026.00	431.95	463.99	1021.06	363.14	414.98	242.06	135.86	135.67	203.09	141.03	135.57
	TIME	0.00	5.19	19.91	8.41	291.42	95.23	295.90	580.98	579.57	496.54	148.83	269.02
10%	PSNR	10.14	20.17	19.91	10.28	22.58	21.76	25.43	30.15	30.16	27.01	30.33	31.80
	SSIM	0.1879	0.4520	0.4480	0.0928	0.7116	0.6370	0.6565	0.8298	0.8297	0.7801	0.8458	0.9137
	FSIM	0.4923	0.7458	0.7174	0.5638	0.7869	0.7771	0.8303	0.8946	0.8946	0.8739	0.8970	0.9267
	ERGAS	998.62	317.70	328.31	982.74	240.31	270.80	178.58	100.56	100.53	146.33	99.06	83.34
	TIME	0.00	5.22	15.14	11.11	262.67	92.75	347.14	618.60	589.45	370.08	157.45	289.08
20%	PSNR	10.66	23.46	24.15	11.14	27.66	26.22	29.22	34.59	34.45	30.88	34.13	35.78
	SSIM	0.2189	0.6402	0.6708	0.1120	0.8742	0.8143	0.8091	0.9374	0.9318	0.8918	0.9364	0.9647
	FSIM	0.5436	0.8242	0.8281	0.5693	0.8988	0.8819	0.8992	0.9531	0.9505	0.9301	0.9462	0.9670
	ERGAS	941.39	216.79	200.76	890.84	134.01	162.07	116.64	60.24	61.20	93.37	63.74	52.71
	TIME	0.00	5.92	14.70	32.14	261.69	96.76	408.08	614.34	610.98	259.80	179.08	316.87
30%	PSNR	11.23	25.92	27.58	11.95	30.87	29.33	32.17	37.99	37.21	33.71	37.59	38.36
	SSIM	0.2531	0.7597	0.8143	0.1441	0.9324	0.8948	0.8883	0.9766	0.9662	0.9399	0.9720	0.9795
	FSIM	0.5753	0.8745	0.8950	0.5803	0.9436	0.9296	0.9384	0.9794	0.9737	0.9583	0.9747	0.9811
	ERGAS	881.07	163.09	134.96	812.92	92.55	113.38	83.48	40.76	44.53	67.19	42.72	39.06
	TIME	0.00	6.62	14.77	91.60	293.70	109.98	494.22	695.60	692.78	223.18	212.90	329.29

SVD, MCPTC and ScadTC methods perform better when the sampling rate increases, but the corresponding images will produce artifacts when the sampling rate decreases. A similar situation also occurs in FTNN method, that is, the recovery

result of FTNN at low sampling rate is also very unsatisfactory. In the meantime, the overall effect of FTNN is quite good with the increase of sampling rate, but there are still some unsatisfactory aspects in local detail information extraction.

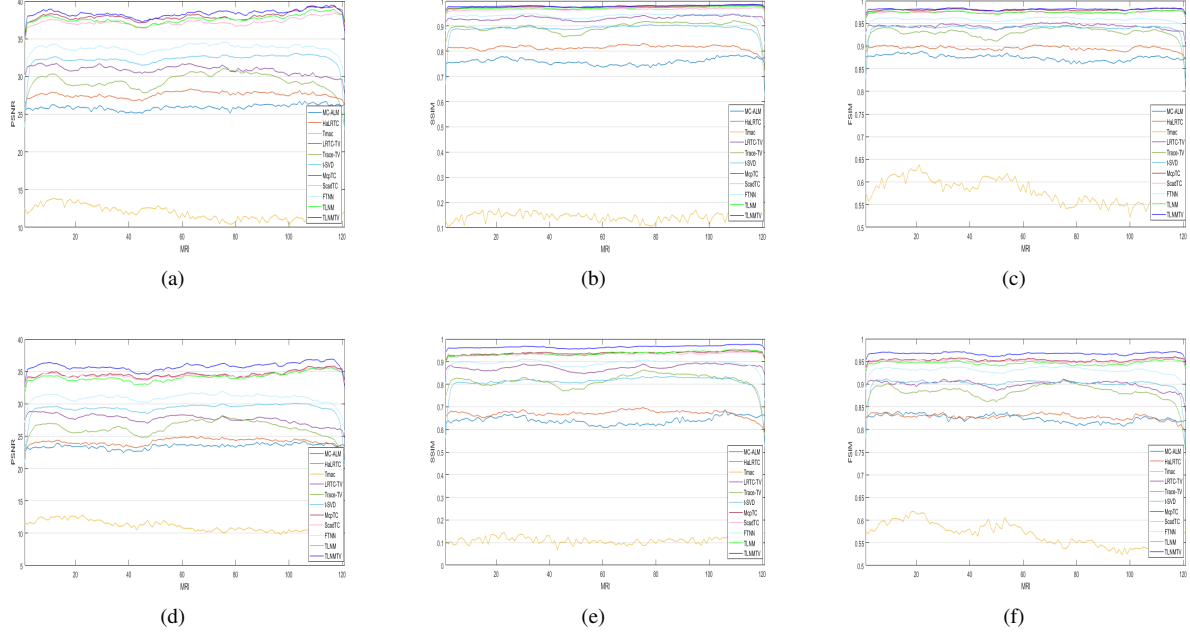


Fig. 8. PSNR, SSIM, and FSIM values comparison of different methods for each slice on MRI data sets, (a)-(c) under SR 30%, (d)-(f) under SR 20%.

TABLE IV
AVERAGE QUANTITATIVE EVALUATION OF THE RESULTS FOR DIFFERENT COLOR VEDIOS WITH SRs 10%

VEDIO	index	Observed	MC-ALM	HaLRTC	TMac	LRTC-TV	McpTC	ScadTC	TLNM	TLNMTV
news	PSNR	8.98	18.84	19.50	9.30	19.07	26.70	26.70	28.77	29.52
	SSIM	0.037	0.531	0.649	0.057	0.670	0.831	0.831	0.846	0.900
	FSIM	0.474	0.745	0.785	0.527	0.765	0.902	0.902	0.912	0.938
	ERGAS	1024.94	329.96	306.34	989.43	328.95	133.93	133.93	106.92	97.70
	TIME	0.00	11.82	79.16	10.19	977.40	1728.38	1757.35	508.39	895.84
akiyo	PSNR	7.37	21.39	22.65	7.69	19.96	34.20	34.20	34.80	35.09
	SSIM	0.025	0.560	0.709	0.038	0.700	0.940	0.940	0.939	0.958
	FSIM	0.461	0.777	0.836	0.472	0.818	0.964	0.964	0.963	0.973
	ERGAS	1100.19	220.82	190.40	1061.93	321.73	50.36	50.36	47.44	45.71
	TIME	0.00	10.89	74.61	8.87	859.76	1716.93	1717.16	508.11	897.09
hall	PSNR	5.93	19.80	21.34	6.25	19.34	29.82	29.82	30.99	31.21
	SSIM	0.016	0.543	0.696	0.023	0.582	0.895	0.895	0.898	0.922
	FSIM	0.404	0.744	0.807	0.463	0.752	0.937	0.937	0.937	0.951
	ERGAS	1152.54	236.88	196.76	1112.04	265.92	75.06	75.06	67.13	64.75
	TIME	0.00	10.91	65.04	11.77	861.41	1705.11	1706.73	499.21	889.17
highway	PSNR	3.62	24.83	25.69	3.94	27.15	31.68	31.59	31.44	32.09
	SSIM	0.011	0.648	0.714	0.015	0.760	0.882	0.877	0.869	0.882
	FSIM	0.391	0.843	0.836	0.368	0.851	0.949	0.947	0.944	0.941
	ERGAS	1320.51	115.15	104.30	1272.99	88.52	52.45	53.02	54.09	50.18
	TIME	0.00	10.92	65.12	12.75	857.97	1705.27	1703.95	503.40	901.32
foreman	PSNR	4.33	18.34	18.89	4.70	21.03	26.53	26.53	27.57	28.02
	SSIM	0.011	0.348	0.457	0.015	0.675	0.787	0.787	0.800	0.835
	FSIM	0.402	0.672	0.695	0.421	0.783	0.867	0.867	0.870	0.886
	ERGAS	1249.48	249.82	234.52	1196.91	184.74	97.47	97.47	87.14	82.54
	TIME	0.00	10.99	61.19	13.25	865.74	1712.17	1712.32	510.28	912.85
container	PSNR	4.88	20.18	21.77	5.26	21.36	29.62	29.62	32.00	32.51
	SSIM	0.011	0.646	0.736	0.017	0.705	0.898	0.897	0.921	0.939
	FSIM	0.390	0.769	0.802	0.419	0.778	0.942	0.942	0.956	0.968
	ERGAS	1207.04	208.37	172.96	1155.94	182.38	70.00	70.03	53.39	50.31
	TIME	0.00	10.99	60.20	20.12	873.43	1729.23	1734.77	530.20	931.37
coastguard	PSNR	6.86	19.80	20.32	7.20	21.74	24.64	24.64	25.13	25.63
	SSIM	0.020	0.405	0.490	0.029	0.545	0.688	0.689	0.699	0.734
	FSIM	0.431	0.731	0.688	0.554	0.676	0.839	0.839	0.857	0.860
	ERGAS	1098.55	249.02	235.51	1056.82	200.52	144.45	144.43	136.85	128.81
	TIME	0.00	10.96	58.56	16.58	880.91	1710.71	1768.39	518.94	930.92

In contrast, our method can obtain fairly accurate results at 5% sampling rates and more accurate results at 10% and 20%

In Tables I-II, we list the numerical results of mean PSNR

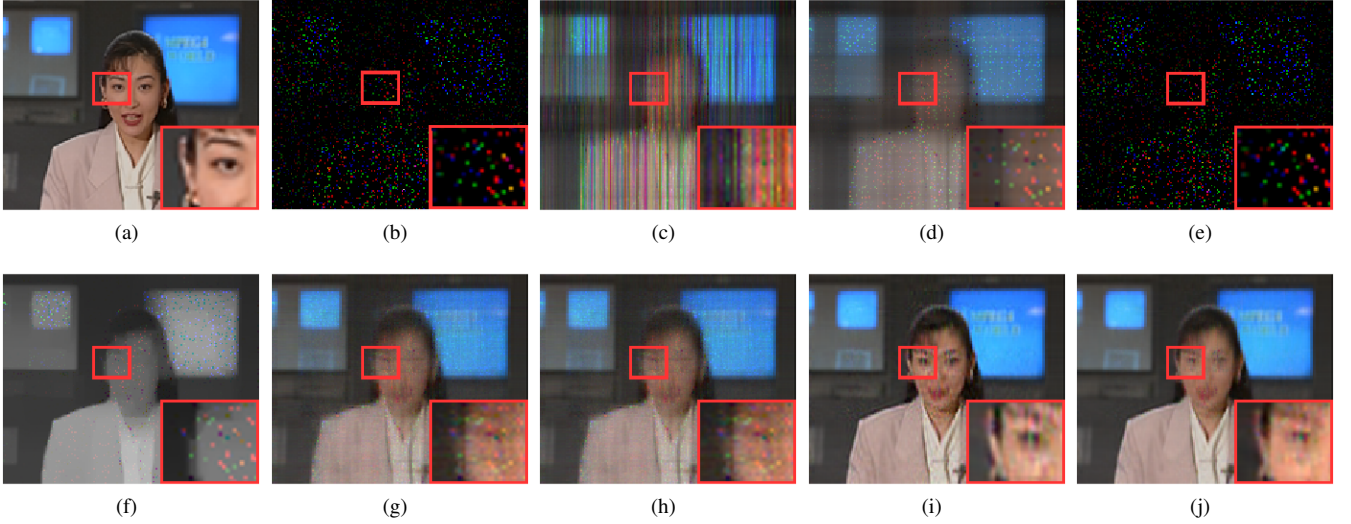


Fig. 9. (a) Original images 140-th frame of akiyo. (b) Corresponding sampled images with SR 5%. (c)-(j) Completed images achieved by six competing methods and proposed TLNM method and TLNMTV method, respectively. (a) Original image. (b) Corrupted image. (c) MC-ALM. (d) HaLRTC. (e) TMac. (f) LRTC-TV. (g) McpTC. (h) ScadTC. (i) TLNM. (j) TLNMTV.

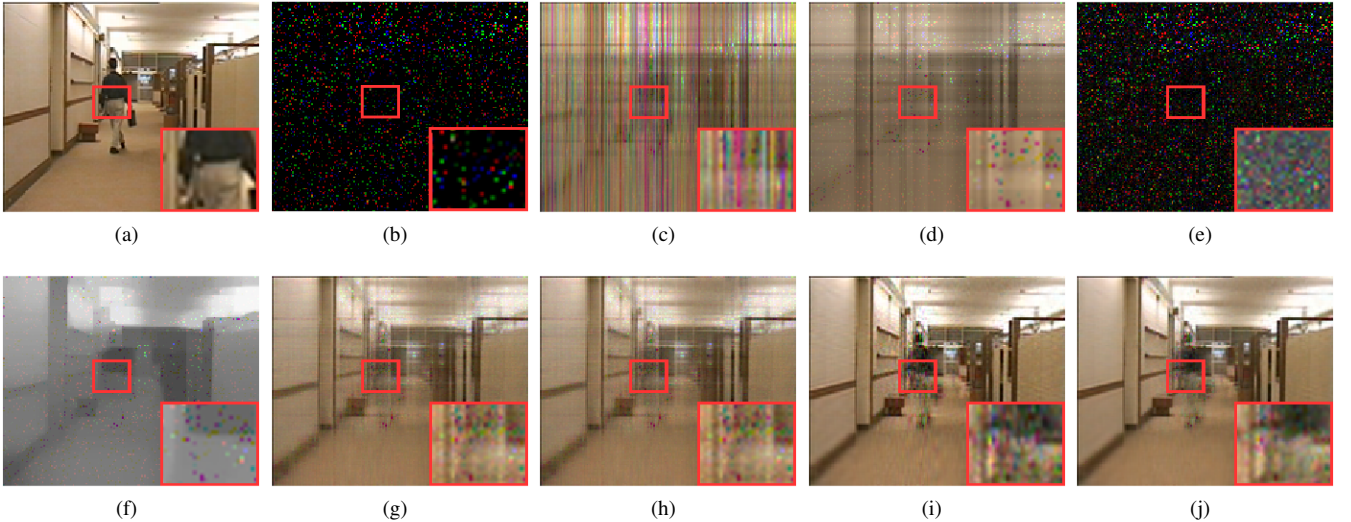


Fig. 10. (a) Original images 60-th frame of hall. (b) Corresponding sampled images with SR 5%. (c)-(j) Completed images achieved by six competing methods and proposed TLNM method and TLNMTV method, respectively. (a) Original image. (b) Corrupted image. (c) MC-ALM. (d) HaLRTC. (e) TMac. (f) LRTC-TV. (g) McpTC. (h) ScadTC. (i) TLNM. (j) TLNMTV.

(MPSNR), mean SSIM (MSSIM), mean FSIM (MFSIM), ERGAS and time consumption (TIME) of all spectral bands of six HSIs under the condition of SR 5% and 10%. To illustrate the advantages of the proposed method, we mainly compare our method with the state of art methods recently developed. First of all, when the sampling rate is 5%, except for the t-SVD method for *cloth*, it only takes 670s, and all other HSIs require more than 1000s. In particular, both the MCPTC and ScadTC methods take more than 1300s for all the images, and the FTNN method costs an average of more than 600 seconds for the six HSI. However, the average time consumed by our TLNM method is about 260s, which is much less than the time required by all the methods mentioned before, and the visual effect of the images obtained at this time exceeds the previous methods. Compared with MCPTC, when SR is 5%

the MPSNR of the TLNM method improved by at least 2.5 dB for *toy*, 2 dB for *flowers* and 4 dB for *beads*, respectively. When the sampling rate is 10%, the time required by the t-SVD, MCPTC, ScadTC methods and our method increases due to the increase of sampling information. It was noted that although the time required by the FTNN method is reduced to a certain extent, compared with our TLNM method, the FTNN method still requires considerably more time. Meantime, the TLNMTV method takes more time than the TLNM method, it produces better visual results. Finally, compared with the TLNM method, the MPSNR index is improved by 1 dB on average for the six HSIs when SR is 5%, and 1.9 dB on average when SR was 10%. The same results from the three image quality indicators MSSIM, MFSIM and ERGAS also verify that TLNMTV is the best.

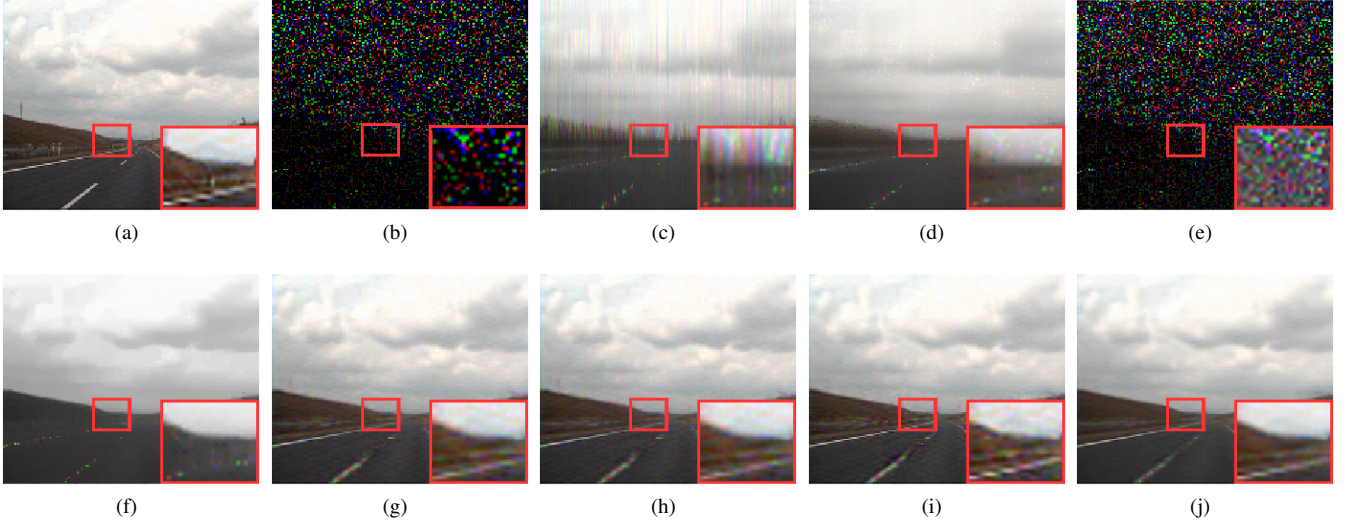


Fig. 11. (a) Original images 110-th frame of highway. (b) Corresponding sampled images with SR 10%. (c)-(j) Completed images achieved by six competing methods and proposed TLNM method and TLNMTV method, respectively. (a) Original image. (b) Corrupted image. (c) MC-ALM. (d) HaLRTC. (e) TMac. (f) LRTC-TV. (g) McpTC. (h) ScadTC. (i) TLNM. (j) TLNMTV.

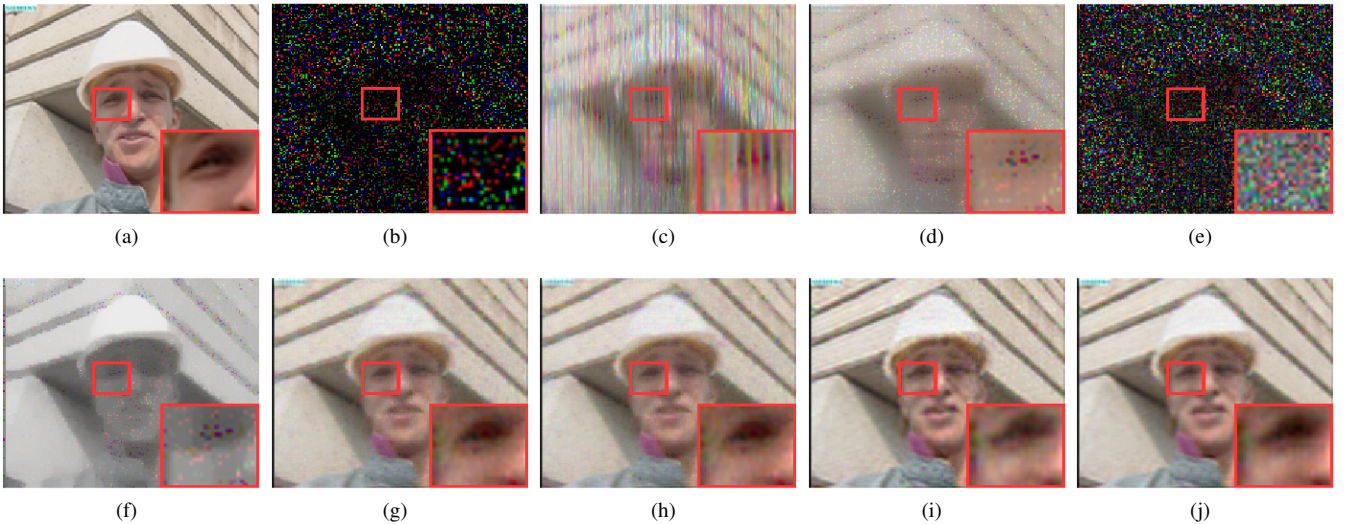


Fig. 12. (a) Original images 60-th frame of foreman. (b) Corresponding sampled images with SR 10%. (c)-(j) Completed images achieved by six competing methods and proposed TLNM method and TLNMTV method, respectively. (a) Original image. (b) Corrupted image. (c) MC-ALM. (d) HaLRTC. (e) TMac. (f) LRTC-TV. (g) McpTC. (h) ScadTC. (i) TLNM. (j) TLNMTV.

It is observed from the actual experimental process that our method can achieve better results at a low sampling rate. In view of this, we have done experiments at a sampling rate of 2.5%. Fig. 4 shows the visual effect at a 2.5% sampling rate, and Fig. 5 further illustrates the performance of all methods on different HSI, showing the MPSNR, MSSIM, and MFSIM of all methods on all HSI. When the sampling rate is 2.5%, it can be seen from the visual effect in Fig. 4 that our method can still obtain more significant restoration effect at a very low sampling rate of 2.5%, which is quite effective in extracting both global visual and structural information and local detail information. And Fig. 5 shows that when the sampling rate is 2.5%, the results obtained by our method are better than those obtained by other state-of-the-art methods.

B. MRI Completion

We test the performance of the proposed method and the comparison method on MRI² data with the size of $181 \times 217 \times 121$. Figs. 6-7 shows the visual effects of MRI images at the sampling rate of 5% and 10%, respectively. Figs. 8 describes the specific values of PSNR, SSIM and FSIM of each slice at the sampling rate of 20% and 30%. As one can see from Figure 8, the TLNMTV methods are all at the top of the line. In addition, the lines of TLNM method and McpTC method are basically close for each slice, it is, however, worth mentioning that our method performs best, followed by McpTC method.

Table III reports the mean PSNR, mean SSIM, mean FSIM, ERGAS, and time values for each sample rate. As the sampling

²http://brainweb.bic.mni.mcgill.ca/brainweb/selection_normal.html

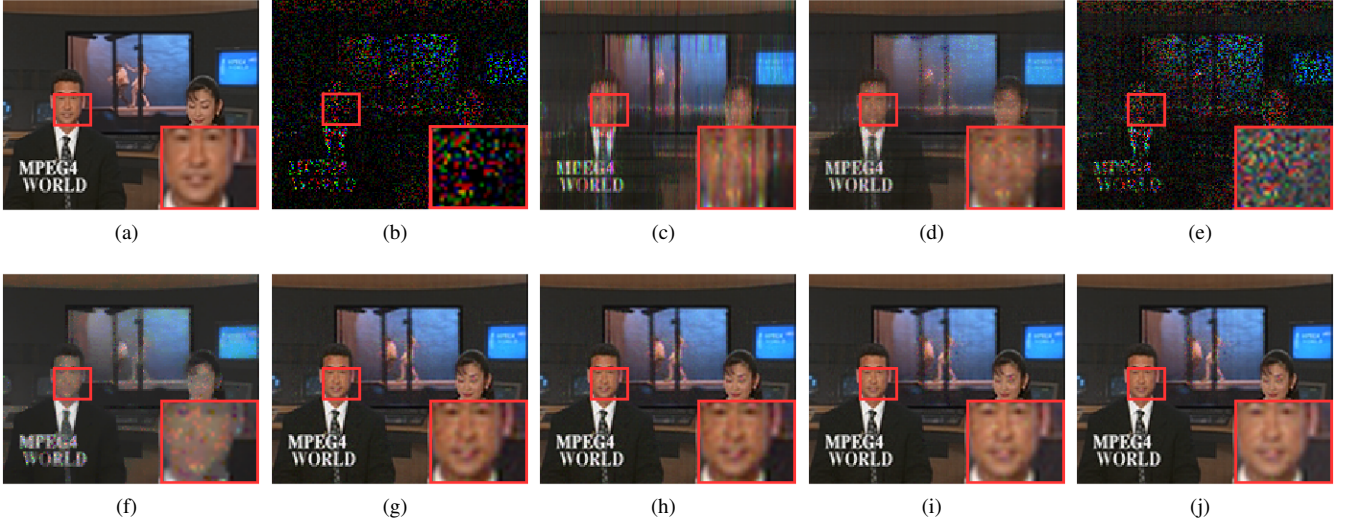


Fig. 13. (a) Original images 70-th frame of news. (b) Corresponding sampled images with SR 20%. (c)-(j) Completed images achieved by six competing methods and proposed TLNM method and TLNMTV method, respectively. (a) Original image. (b) Corrupted image. (c) MC-ALM. (d) HaLRTC. (e) TMac. (f) LRTC-TV. (g) McpTC. (h) ScadTC. (i) TLNM. (j) TLNMTV.

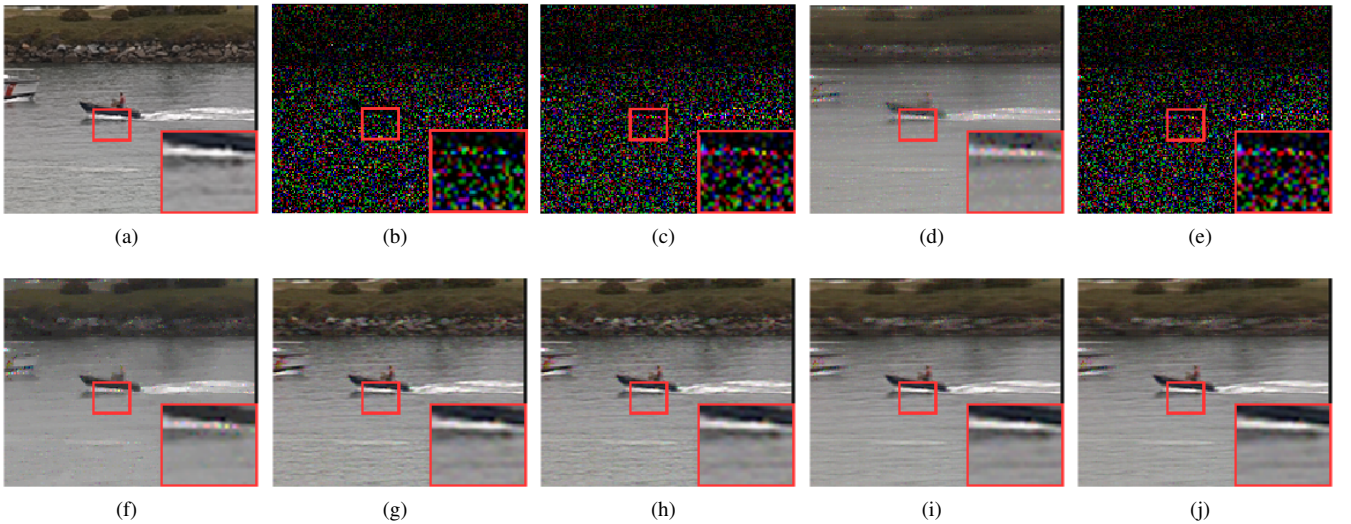


Fig. 14. (a) Original images 10-th frame of container. (b) Corresponding sampled images with SR 20%. (c)-(j) Completed images achieved by six competing methods and proposed TLNM method and TLNMTV method, respectively. (a) Original image. (b) Corrupted image. (c) MC-ALM. (d) HaLRTC. (e) TMac. (f) LRTC-TV. (g) McpTC. (h) ScadTC. (i) TLNM. (j) TLNMTV.

rate increases and the sampling information increases, the preset value of r in our method increases accordingly. The analysis in the computational complexity section shows that our method increases as r increases. So as the sampling rate increases, the time we spend will increase. As can be seen from Table III, our TLNM method is only 0.2dB lower than the result of McpTC method at each sampling rate, but the shortest time required by TLNM method is 141s and the highest time is 212s, while the McpTC method requires 600s, far more than the TLNM method. The time required by our TLNMTV method is 270 to 330 seconds, which is more time-consuming than TLNM method, but the MPSNR, MSSIM and MFSIM results are higher than other methods. Compared with McpTC, the corresponding MPSNR value was improved by nearly 1dB.

C. Color Video Completion

In this subsection, seven color videos³ (respectively named "news", "akiyo", "hall", "highwayf", "foreman", "container", "coastguard") with the size $144 \times 176 \times 3 \times 150$ are selected as the ground truth fourth-order data. Six methods, namely MC-ALM, HaLRTC, TMac, LRTC-TV, McpTC and ScadTC, are used for color video to demonstrate the superiority of our method. The amount of data information of color video data is greater than the previous two types of data. Our TLNM method can restore the visual effect of the image effectively, and still has faster speed. Table IV shows the average quantitative evaluation of each frame of video data with different colors when the sampling rate is 10%. Figs. 9-14 show the visual

³<http://trace.eas.asu.edu/yuv/>

effects of different frames of different color videos. It can be seen from all these figures that our method is superior to all comparative methods mentioned in terms of overall recovery effect and detailed information extraction.

V. CONCLUSION

In this paper, $L_{2,1}$ norm minimization model and CSVD-QR method are used to solve the tensor complete problem, and the direct calculation of SVD decomposition is avoided fundamentally, and a good approximation of nuclear norm is given based on CSVD-QR method. This provides a new way of thinking and method skills for solving the tensor restoration problem more accurately and quickly. Experiments on three tensor-complete data sets, namely hyperspectral images, magnetic resonance images and color video, show that the proposed TLNM method has a super fast speed, and the improved TLNMTV method greatly improves the solution accuracy under the condition of increasing a certain amount of time, that is, high quality restoration effect. It is especially worth emphasizing that our method can still complete the missing term recovery of HSI well when the SR is 2.5% or even lower. In the future work, we will try to consider how to use the latest TV or other variant technology to improve the visual effect more reasonably on the premise of ensuring the speed of the method's growth is relatively small.

REFERENCES

- [1] Q. Liu, F. Davoine, J. Yang, Y. Cui, Z. Jin, and F. Han, "A fast and accurate matrix completion method based on qr decomposition and $l_{2,1}$ -norm minimization," *IEEE Transactions on Neural Networks and Learning Systems*, vol. 30, no. 3, pp. 803–817, 2019.
- [2] J. Xue, Y. Zhao, W. Liao, and J. Cheung-Wai Chan, "Nonconvex tensor rank minimization and its applications to tensor recovery," *Information Sciences*, vol. 503, pp. 109–128, 2019.
- [3] L. Zhang, L. Zhang, D. Tao, and X. Huang, "Tensor discriminative locality alignment for hyperspectral image spectral-spatial feature extraction," *IEEE Transactions on Geoscience and Remote Sensing*, vol. 51, no. 1, pp. 242–256, 2013.
- [4] Q. Li and D. Schonfeld, "Multilinear discriminant analysis for higher-order tensor data classification," *IEEE Transactions on Pattern Analysis and Machine Intelligence*, vol. 36, no. 12, pp. 2524–2537, 2014.
- [5] X. Cao, X. Wei, Y. Han, and D. Lin, "Robust face clustering via tensor decomposition," *IEEE Transactions on Cybernetics*, vol. 45, no. 11, pp. 2546–2557, 2015.
- [6] J. Xue, Y. Zhao, W. Liao, J. C.-W. Chan, and S. G. Kong, "Enhanced sparsity prior model for low-rank tensor completion," *IEEE Transactions on Neural Networks and Learning Systems*, vol. 31, no. 11, pp. 4567–4581, 2020.
- [7] J. Xue, Y. Zhao, W. Liao, and J. C.-W. Chan, "Nonlocal low-rank regularized tensor decomposition for hyperspectral image denoising," *IEEE Transactions on Geoscience and Remote Sensing*, vol. 57, no. 7, pp. 5174–5189, 2019.
- [8] E. Acar, D. M. Dunlavy, T. G. Kolda, and M. Mørup, "Scalable tensor factorizations for incomplete data," *Chemometrics and Intelligent Laboratory Systems*, vol. 106, no. 1, pp. 41–56, 2011.
- [9] P. Tichavský, A.-H. Phan, and A. Cichocki, "Numerical cp decomposition of some difficult tensors," *Journal of Computational and Applied Mathematics*, vol. 317, pp. 362–370, 2017.
- [10] R. Harshman, "Foundations of the parafac procedure: Model and conditions for an 'explanatory' multi-mode factor analysis," *UCLA Work. Pap. Phon.*, vol. 16, 11 1969.
- [11] L. Tucker, "Some mathematical notes on three-mode factor analysis," *Psychometrika*, vol. 31, pp. 279–311, 02 1966.
- [12] W. Cao, Y. Wang, J. Sun, D. Meng, C. Yang, A. Cichocki, and Z. Xu, "Total variation regularized tensor rpca for background subtraction from compressive measurements," *IEEE Transactions on Image Processing*, vol. 25, no. 9, pp. 4075–4090, 2016.
- [13] M. E. Kilmer and C. D. Martin, "Factorization strategies for third-order tensors," *Linear Algebra and its Applications*, vol. 435, no. 3, pp. 641–658, 2011.
- [14] Z. Zhang, G. Ely, S. Aeron, N. Hao, and M. Kilmer, "Novel methods for multilinear data completion and de-noising based on tensor-svd," *2014 IEEE Conference on Computer Vision and Pattern Recognition*, pp. 3842–3849, 2014.
- [15] C. J. Hillar and L.-H. Lim, "Most tensor problems are np-hard," *Journal of the ACM (JACM)*, vol. 60, no. 6, pp. 1–39, 2013.
- [16] Y.-F. Li, K. Shang, and Z.-H. Huang, "Low Tucker rank tensor recovery via admm based on exact and inexact iteratively reweighted algorithms," *Journal of Computational and Applied Mathematics*, vol. 331, pp. 64–81, 2018.
- [17] X. Li, M. K. Ng, G. Cong, Y. Ye, and Q. Wu, "Mr-ntd: Manifold regularization nonnegative Tucker decomposition for tensor data dimension reduction and representation," *IEEE Transactions on Neural Networks and Learning Systems*, vol. 28, no. 8, pp. 1787–1800, 2017.
- [18] J. Liu, P. Musialski, P. Wonka, and J. Ye, "Tensor completion for estimating missing values in visual data," *IEEE Transactions on Pattern Analysis and Machine Intelligence*, vol. 35, no. 1, pp. 208–220, 2013.
- [19] N. Paragios, Y. Chen, and O. Faugeras, *Handbook of Mathematical Models in Computer Vision II Total Variation Image Restoration: Overview and Recent Developments*. Springer Science & Business Media, 2006, vol. 10.1007/0-387-28831-7, no. Chapter 2.
- [20] X. Cao, L. Yang, and X. Guo, "Total variation regularized rpca for irregularly moving object detection under dynamic background," *IEEE Transactions on Cybernetics*, vol. 46, no. 4, pp. 1014–1027, 2016.
- [21] J. Xue, Y. Zhao, W. Liao, and J. Cheung-Wai Chan, "Total variation and rank-1 constraint rpca for background subtraction," *IEEE Access*, vol. 6, pp. 49 955–49 966, 2018.
- [22] B. Madathil and S. N. George, "Twist tensor total variation regularized-reweighted nuclear norm based tensor completion for video missing area recovery," *Information Sciences*, vol. 423, pp. 376–397, 2018.
- [23] H. Wang, F. Nie, and H. Huang, "Low-rank tensor completion with spatio-temporal consistency," *Proceedings of the Twenty-Eighth AAAI Conference on Artificial Intelligence*, vol. 4, pp. 2846–2852, 01 2014.
- [24] Y. Xu, R. Hao, W. Yin, and Z. Su, "Parallel matrix factorization for low-rank tensor completion," *Inverse Problems and Imaging*, vol. 9, pp. 601–624, 2015.
- [25] X. Li, Y. Ye, and X. Xu, "Low-rank tensor completion with total variation for visual data inpainting," *Proceedings of the Thirty-First AAAI Conference on Artificial Intelligence*, pp. 2210–2216, 2017.
- [26] X. Guo and Y. Ma, "Generalized tensor total variation minimization for visual data recovery?" *2015 IEEE Conference on Computer Vision and Pattern Recognition (CVPR)*, pp. 3603–3611, 2015.
- [27] T. G. Kolda and B. W. Bader, "Tensor decompositions and applications," *SIAM review*, vol. 51, no. 3, pp. 455–500, 2009.
- [28] G. Liu, Z. Lin, and Y. Yu, "Robust subspace segmentation by low-rank representation," *ICML 2010 - Proceedings, 27th International Conference on Machine Learning*, pp. 663–670, 08 2010.
- [29] J.-F. Cai, E. J. Candès, and Z. Shen, "A singular value thresholding algorithm for matrix completion," *SIAM Journal on Optimization*, vol. 20, no. 4, pp. 1956–1982, 2010.
- [30] Z. Wang, A. Bovik, H. Sheikh, and E. Simoncelli, "Image quality assessment: from error visibility to structural similarity," *IEEE Transactions on Image Processing*, vol. 13, no. 4, pp. 600–612, 2004.
- [31] L. Zhang, L. Zhang, X. Mou, and D. Zhang, "Fsim: A feature similarity index for image quality assessment," *IEEE Transactions on Image Processing*, vol. 20, no. 8, pp. 2378–2386, 2011.
- [32] L. Wald, *Data fusion: definitions and architectures: fusion of images of different spatial resolutions*. Presses des MINES, 01 2002.
- [33] Z. Zhang and S. Aeron, "Exact tensor completion using t-svd," *IEEE Transactions on Signal Processing*, vol. 65, no. 6, pp. 1511–1526, 2017.
- [34] Z. Lin, M. Chen, and Y. Ma, "The augmented lagrange multiplier method for exact recovery of corrupted low-rank matrices," *Mathematical Programming*, vol. 9, 09 2010.
- [35] D. Goldfarb and Z. Qin, "Robust low-rank tensor recovery: Models and algorithms," *SIAM Journal on Matrix Analysis and Applications*, vol. 35, no. 1, pp. 225–253, 2014.
- [36] T.-X. Jiang, M. K. Ng, X.-L. Zhao, and T.-Z. Huang, "Framelet representation of tensor nuclear norm for third-order tensor completion," *IEEE Transactions on Image Processing*, vol. 29, pp. 7233–7244, 2020.
- [37] M. M, H. LK, and A. SM, "Algorithms for sparse nonnegative Tucker decompositions," *Neural computation*, vol. 20, no. 8, pp. 2112–2131, 1 2008.